

# Synthesis and Characterization of a Biocompatible Nanoplatfom Based on Silica-Embedded SPIONs Functionalized with Polydopamine

Miriam Romano, Manuel Antonio González Gómez, Pamela Santonicola, Noemi Aloj, Svenja Offer, Jana Pantzke, Samuele Raccosta, Valeria Longo, Alessandro Surpi, Silvia Alacqua, Giuseppina Zampi, Valentin Alek Dediu, Bernhard Michalke, Ralf Zimmerman, Mauro Manno, Yolanda Piñeiro, Paolo Colombo, Elia Di Schiavi, José Rivas, Paolo Bergese, and Sebastiano Di Bucchianico\*



Cite This: <https://doi.org/10.1021/acsbomaterials.2c00946>



Read Online

ACCESS |



Metrics & More



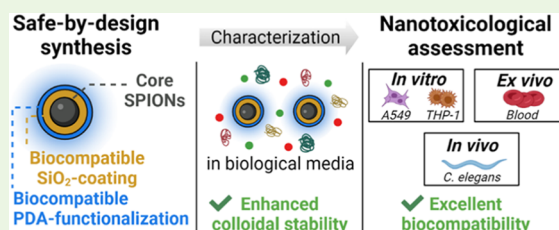
Article Recommendations



Supporting Information

**ABSTRACT:** Superparamagnetic iron oxide nanoparticles (SPIONs) have gained increasing interest in nanomedicine, but most of those that have entered the clinical trials have been withdrawn due to toxicity concerns. Therefore, there is an urgent need to design low-risk and biocompatible SPION formulations. In this work, we present an original safe-by-design nanoplatfom made of silica nanoparticles loaded with SPIONs and decorated with polydopamine (SPIONs@SiO<sub>2</sub>-PDA) and the study of its biocompatibility performance by an ad hoc thorough in vitro to in vivo nanotoxicological methodology. The results indicate that the SPIONs@SiO<sub>2</sub>-PDA have excellent colloidal stability in serum-supplemented culture media, even after long-term (24 h) exposure, showing no cytotoxic or genotoxic effects in vitro and ex vivo. Physiological responses, evaluated in vivo using *Caenorhabditis elegans* as the animal model, showed no impact on fertility and embryonic viability, induction of an oxidative stress response, and a mild impact on animal locomotion. These tests indicate that the synergistic combination of the silica matrix and PDA coating we developed effectively protects the SPIONs, providing enhanced colloidal stability and excellent biocompatibility.

**KEYWORDS:** SPION, silica, coating materials, polydopamine, nanotoxicity, *C. elegans*



## INTRODUCTION

Superparamagnetic iron oxide nanoparticles (SPIONs) are among the most investigated magnetic nanoparticles (MNPs) due to their high responsivity to magnetic fields. Namely, SPIONs possess null magnetic remanence combined with high-saturation magnetization that assures no inter-particle magnetic interactions in the absence of external magnetic fields and a fast and robust response when the latter is applied.<sup>1</sup> This characteristic fundamentally opens up broad horizons for their use in guided and controllable nanoparticle (NP) targeting and activity under magnetic fields. Being easily manageable by using external fields, SPIONs have gained interest in a wide range of applications, from magnetic resonance imaging (MRI)<sup>2</sup> to cell/tissue targeting or magnetic hyperthermia treatment (MHT).<sup>3</sup> SPIONs' architecture is mainly based on maghemite ( $\gamma$ -Fe<sub>2</sub>O<sub>3</sub>) or magnetite (Fe<sub>3</sub>O<sub>4</sub>) cores covered by an external coating<sup>4</sup> which steers NP interactions within the biological environment. SPION surface coatings provide augmented colloidal stability,<sup>5</sup> and several efforts have been attempted to design and synthesize clinical-ready low-risk SPIONs coated with biocompatible shells mostly made of dextran or dextran derivatives (e.g., Endorem or Resovist).<sup>6,7</sup> In general, the nature of the surface shells (along with their

size) represents a key factor in determining SPION uptake, toxicity,<sup>8</sup> and biodistribution profiles.<sup>4,9,10</sup> In this regard, silica (SiO<sub>2</sub>) and bioinspired polydopamine (PDA) coatings can endow SPIONs with interesting biological and optical properties. From a biological standpoint, it has already been demonstrated that silica shells can lessen SPION cytotoxic effects by preventing corrosion and inhibiting iron ion release.<sup>11</sup> On the other hand, PDA emerged as a promising NP coating material due to its natural origin.<sup>12</sup> Furthermore, PDA is highly reactive and can be used to increase NPs' drug binding/loading processes and release efficiencies,<sup>13</sup> making it feasible for drug delivery in targeted therapies. Both silica-embedded and PDA-functionalized SPIONs have already been applied in several in vitro and in vivo pre-clinical studies for their use as drug delivery systems,<sup>14,15</sup> MHT,<sup>16</sup> and MRI

Received: August 11, 2022

Accepted: November 28, 2022

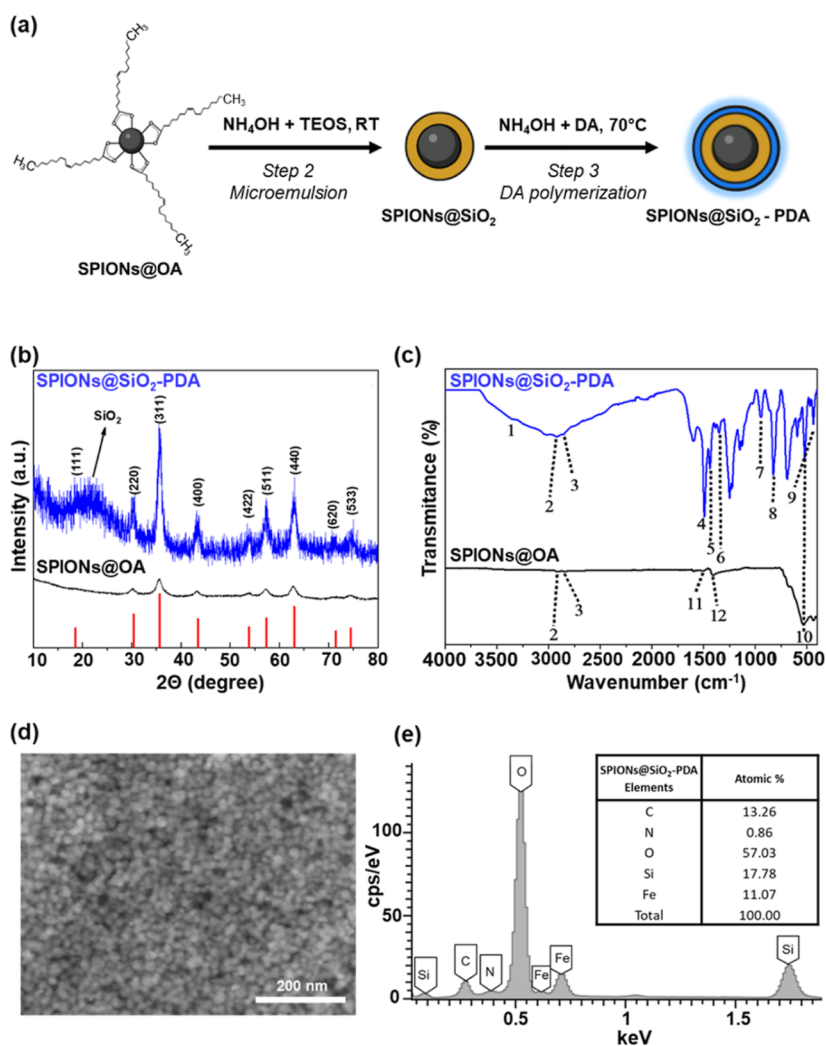


**Figure 1.** Demonstration of silica coating and polydopamine functionalization. (a) Scheme of the synthetic protocol used to obtain SPIONs@SiO<sub>2</sub>-PDA; (b) XRD patterns of SPIONs@OA (black pattern) and SPIONs@SiO<sub>2</sub>-PDA (blue pattern) compared to the XRD pattern of magnetite from the ICDD no. 00-019-629 database; (c) FTIR spectra of the SPIONs@OA (black pattern) and SPIONs@SiO<sub>2</sub>-PDA (blue pattern), with the characteristic bands of 1 =  $\nu_{\text{NH}_2}$ , 2 =  $\nu_{\text{asCH}_2}$ , 3 =  $\nu_{\text{sCH}_2}$ , 4 =  $\nu_{\text{C=N}}$ , 5 =  $\delta_{\text{NH}_2}$ , 6 =  $\nu_{\text{C-N-C}}$ , 7 =  $\nu_{\text{as Si-O-Si}}$ , 8 =  $\nu_{\text{s Si-O-Si}}$ , 9 =  $\delta_{\text{Si-O-Si}}$ , 10 =  $\nu_{\text{FeO}}$ , 11 =  $\nu_{\text{as COO}}$ , and 12 =  $\nu_{\text{s COO}}$ ; (d) FESEM image; (e) FESEM-EDX elemental composition spectrum of SPIONs@SiO<sub>2</sub>-PDA.

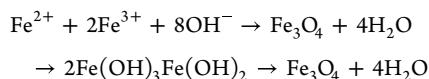
agents.<sup>17,18</sup> Furthermore, PDA manifests UVA-induced fluorescence,<sup>19</sup> which can provide silica-coated SPIONs with distinct optical properties exploitable for in vitro or ex vivo fluorescence analysis.

PDA coating is usually made through PDA-self polymerization by immersing NPs in a dopamine alkaline aqueous solution.<sup>12</sup> Despite being considered a gold-standard method, several parameters like temperature and pH can affect the coating efficiency of this process,<sup>13,20</sup> leading to high-grade batch-to-batch variability. Furthermore, chemical residues from Tris hydrochloride—commonly used to create an alkaline environment<sup>13</sup>—can contribute to unexpected toxic side effects. In this case, a different safe-by-design approach can help reduce risks, safeguarding SPIONs' synthetic reproducibility. Here, we present a novel nanoplatform made of silica nanoparticles loaded with SPIONs and functionalized with polydopamine (SPIONs@SiO<sub>2</sub>-PDA) by a biocompatible, highly reproducible, and cost-effective procedure. We also provide extensive, stepwise, biological, and nanotoxicological characterization in vitro, ex vivo, and in vivo, as required in the minimum information reporting in bio-nano experimental

literature.<sup>21</sup> SPIONs@SiO<sub>2</sub>-PDA biocompatibility was assessed by a broad set of toxicological assays in vitro in the A549 cancerous alveolar epithelial lung cell line and in monocyte/macrophage THP-1 cells, ex vivo in whole human blood, and in vivo using *Caenorhabditis elegans* as an animal model fulfilling the 3R principles (replacement, reduction, and refinement). Throughout all three biological characterization steps, we observed no cytotoxicity or genotoxicity and mild effects in vivo on animal locomotion. Responsiveness to external magnetic fields and SPIONs@SiO<sub>2</sub>-PDA's capability to be effectively concentrated in sub-millimeter-sized regions by external magnets confirmed their potential for future theranostic applications.

## ■ MATERIALS AND METHODS

**Synthesis of Silica-Embedded SPIONs Functionalized with Polydopamine (SPIONs@SiO<sub>2</sub>-PDA).** SPIONs@SiO<sub>2</sub>-PDA were obtained using three synthetic steps, including co-precipitation, microemulsion, and polymerization (Figure 1a). Step 1 led to the production of iron oxide NPs coated with oleic acid (SPIONs@OA) by co-precipitation, according to the reaction equation



Keeping the molar ratio 1:2 for total precipitation of  $\text{Fe}_3\text{O}_4$  in a reducing environment, as described in González-Gómez et al.,<sup>22</sup> with some modifications related to the washing procedure of the obtained hydrophobic MNPs (S1). In step 2, SPIONs@OA were coated with silica (SPIONs@SiO<sub>2</sub>) by a water-in-cyclohexane reverse micro-emulsion process, as reported by Moldes-Diz et al.<sup>23</sup> Experimental details can be found in S1. SPIONs@SiO<sub>2</sub> were washed four times using 2-propanol (IPA, C<sub>3</sub>H<sub>8</sub>O). SPIONs@SiO<sub>2</sub> were retained with a permanent magnet for each wash, and the supernatant was removed. SPIONs@SiO<sub>2</sub> were washed twice with Milli-Q water, centrifuged at 9000 rpm for 15 min, and redispersed in Milli-Q water. Finally, step 3 led to the functionalization of SPIONs@SiO<sub>2</sub> with polydopamine (SPIONs@SiO<sub>2</sub>-PDA) based on the dopamine polymerization on SPIONs@SiO<sub>2</sub>. First, SPIONs@SiO<sub>2</sub> (31 mg) were dispersed in 10 mL of Milli-Q water. Then NH<sub>4</sub>OH (1 mmol) and dopamine hydrochloride (DA, C<sub>8</sub>H<sub>11</sub>NO<sub>2</sub>·HCl, 0.19 mmol) were added and incubated at 70 °C overnight. SPIONs@SiO<sub>2</sub>-PDA were separated from the reaction medium by a magnetic field and washed six times with Milli-Q water. Finally, SPIONs@SiO<sub>2</sub>-PDA were re-dispersed in Milli-Q water to a final concentration of 0.1 % wt (256 μg) determined by thermogravimetric analysis (TGA) and flame atomic absorption spectroscopy (FAAS). All solvents and chemicals were of analytical grade and purchased from Sigma-Aldrich.

**Physicochemical, Optical, and Magnetic Characterization of SPIONs@SiO<sub>2</sub>-PDA.** X-ray diffraction was performed with an X-ray diffractometer using a Philips PW1710 diffractometer (Panalytical) operated at 40 kV and 30 mA, and the spectrum was recorded by Cu K $\alpha$  radiation source ( $\lambda = 1.54186 \text{ \AA}$ ). Measurements were collected in the  $2\theta$  angle range between 10 and 80° with steps of 0.02° and 10 s/step. Surface functional groups of dried SPIONs were analyzed by Fourier transform infrared (FTIR) spectroscopy with a Thermo Nicolet Nexus spectrometer (Thermo Fisher Scientific) using the attenuated total reflectance method from 4000 to 400 cm<sup>-1</sup>. The morphology and size were studied by transmission electron microscopy (TEM) using a JEOL JEM-1011 microscope operating at 100 kV. Samples were placed on copper grids with Formvar films for analysis, and the diameter was measured using ImageJ software. The energy dispersive X-ray spectroscopy (EDX) was carried out by a Zeiss Gemini 450 field emission scanning electron microscope, FESEM, (detector EDX model Ultim Extreme, Oxford). The results were acquired at the operating conditions of 5 kV and a working distance of 5 nm. The samples were assembled onto aluminum stubs using conductive double-sided adhesive carbon tabs (Pro SciTech). Iron content in the MNP samples was determined by FAAS performed using an atomic absorption spectrometer (PerkinElmer 3110, Perkin). The composition of the samples was analyzed with a TGA PerkinElmer model 8000 (Perkin). SPIONs@SiO<sub>2</sub>-PDA fluorescence was acquired using a Leica TCS SP8 SMD confocal microscope equipped with an HC PL APO CS 63 × 1.40 OIL objective and a 54.4% 405 nm laser (1024 × 1024-pixel images, bidirectional scan direction). SPIONs@SiO<sub>2</sub>-PDA's magnetic properties were measured by using a vibrating sample magnetometer (DMS/ADE Technologies) and a superconducting quantum interference device magnetometer (Quantum Design, model MPMS-5). Magnetization data were normalized to the magnetic mass (Wmag) amount for each sample (determined by TGA). A microscope-connected CCD camera (Dino-Lite Pro, AnMo Electronics Corporation, Hsinchu City, Taiwan) has been used to follow the behavior of SPION solutions contained inside 500 μm wide quartz capillaries (WJM-Glass/Müller GmbH, Berlin, Germany) under the influence of the magnetic field. A 0.9 mm wide tubing in medical-grade silicon (Silastic Rx 50 medical grade tubing, Dow Corning, Midland, Michigan, USA) connected to a peristaltic pump (120 s, Watson Marlow, Cheltenham, UK) fed the capillary with nanoparticle solutions.

**Cell Culture.** A549 cells (ATCC; CCL-185) were cultured in high-glucose Dulbecco's Modified Eagle Medium: Nutrient Mixture F-12 (DMEM:F-12) (Thermo Fisher Scientific, 31331-028) supplemented with 5% (vol/vol) fetal bovine serum (FBS) (Thermo Fisher Scientific, 10500-064) and 100 U/mL penicillin and 100 μg/mL streptomycin (P/S; Sigma-Aldrich, P4333) hereafter referred to as completeDMEM:F12 media (cDMEM:F12). The human monocytic leukemia THP-1 cell line (ECACC 88081201) was maintained in culture with RPMI 1640 medium (Gibco, Life Technologies, 52400-025) supplemented with heat-inactivated 10% FBS (Gibco, Life Technologies, 10270-106) and 1% P/S (Gibco, Life Technologies, 15070-063), hereafter referred to as completeRPMI (cRPMI). Differentiated THP-1 monocytes with the macrophage-like phenotype M0 (THP-1 M0) were obtained by treating cells with 200 nM phorbol 12-myristate-13-acetate (PMA; Sigma, P8139) for 72 h. A549 and THP-1 cells were maintained in a humidified incubator at 37 °C in 5% carbon dioxide (CO<sub>2</sub>).

**Dynamic Light Scattering Measurements in Culture Media.** SPIONs@SiO<sub>2</sub>-PDA fresh aliquot (1 mg/mL) was vortexed for 3 min and then centrifuged at 4 °C for 10 min at 1000 g. 50 μg/mL SPIONs@SiO<sub>2</sub>-PDA dispersions were prepared in the following buffers: (i) Milli-Q H<sub>2</sub>O, (ii) RPMI + 1% P/S [RPMI], (iii) cRPMI, (iv) DMEM:F12 + 1% P/S [DMEM:F12], (v) cDMEM:F12. Samples were put into quartz cuvettes and incubated at 37 °C for 0, 4, and 24 h. The cells were transferred in a cell compartment of a BI200-SM goniometer (Brookhaven Instruments), thermostated at 20 °C, and equipped with a He-Ne laser (JDS Uniphase 1136P) with wavelength  $\lambda = 633 \text{ nm}$  and a single-pixel photon counting module (Hamamatsu C11202-050). Scattered light intensity and its autocorrelation function  $g_2(t)$  were measured simultaneously at a scattering angle  $\theta = 90^\circ$  using a BI-9000 correlator (Brookhaven Instruments). The electric field autocorrelation function  $g_1(t)$  was calculated by using the Siegert relation

$$g_2(t) = 1 + \beta |g_1(t)|^2 \quad (1)$$

where  $\beta$  is an instrumental parameter<sup>24</sup> and  $g_1(t)$  is the field autocorrelation function, associated with the size ( $\sigma$ ) of diffusing particles and their size distribution [ $P_q(\sigma)$ ] by the relation

$$g_1(t) = \int P_q(\sigma) \exp\{-D(\sigma)q^2t\} d\sigma \quad (2)$$

where  $q = 4\pi\hat{n}\lambda^{-1}\sin(\theta/2)$  is the scattering vector in a medium with  $\hat{n}$  refractive index and  $D(\sigma)$  is the diffusion coefficient of a particle of hydrodynamic diameter  $D_h = \sigma$ , determined by the Stokes-Einstein relation  $D(\sigma) = k_B T [3\pi\eta\sigma]^{-1}$ , with  $T$  being the temperature,  $\eta$  the medium viscosity, and  $k_B$  the Boltzmann constant. The refractive indexes ( $\hat{n}$ ) of each medium were measured by using an Abbe refractometer and taken as (i) 1.3320, (ii) 1.3346, (iii) 1.3350, (iv) 1.3347, and (v) 1.3355. The medium viscosities ( $\eta$ ) were calculated by interpolating the value reported in ref.<sup>25</sup> and taken as (i) 1.002, (ii) 1.111, (iii) 1.311, (iv) 1.115, and (v) 1.457. The size distribution  $P_q(\sigma)$  was calculated by assuming that the diffusion coefficient distribution was shaped as a Schultz distribution, which is a two-parameter asymmetric distribution, determined by the average diffusion coefficient  $\langle D \rangle$  and its variance  $V$ .<sup>26,27</sup> Two robust parameters are derived from this analysis:  $D_z$ , the  $z$ -averaged hydrodynamic diameter (the diameter corresponding to the average diffusion coefficient  $\langle D \rangle$ ), and PDI, the polydispersity index (here calculated as  $\text{PDI} = V/\langle D \rangle^2$ ), an estimation of the distribution width. The buffers containing FBS displayed a non-null intensity autocorrelation function due to the presence of several NPs. In this case, the field autocorrelation function of the medium  $g_1^M(t)$  was measured, and then the NP autocorrelation function  $g_1^{\text{NP}}(t)$  was calculated by a forced fit, fixing the medium component

$$|g_1(t)|^2 = \alpha |g_1^M(t)|^2 + (1 - \alpha) |g_1^{\text{NP}}(t)|^2 \quad (3)$$

where  $\alpha = 0.95$  is the fraction of integer medium in the sample.<sup>28,29</sup> Preparation of SPIONs@SiO<sub>2</sub>-PDA dispersions in culture media and cell treatments.

For A549 cell treatments, SPIONs@SiO<sub>2</sub>-PDA solutions (1 mg/mL) were vortexed for 3 min at the highest speed using the Advanced IR Vortex Mixer Zx4 (VELP Scientifica) and diluted 1:10 in DMEM/F12 with GlutaMAX, with or without 5% FBS. The 1:10 dilution was sonicated for 1 min with the Pals sonic ultrasonic cleaner (ALLPAX Germany), and finally, the suspensions were diluted to their final concentrations and immediately used for cell exposures. For THP-1 M0 cell treatments, SPIONs@SiO<sub>2</sub>-PDA solutions (1 mg/mL) were vortexed and resuspended as described above in cRPMI 1640 medium and immediately used for cell treatment. A549 and THP-1 M0 cell treatments were carried out in 24-well (Corning, 3524) and 96-well (Corning, 3598) tissue culture plates, respectively, and cells were exposed to SPIONs@SiO<sub>2</sub>-PDA dispersions in four different concentrations ranging from 0.1 μg/mL up to 50 μg/mL (corresponding to a range of 0.3–13.16 μg/cm<sup>2</sup> for A549 and 1.8–78.96 μg/cm<sup>2</sup> for THP-1 M0). For A549 exposures, cells were seeded at 3.5 × 10<sup>4</sup> cells/cm<sup>2</sup> in cDMEM/F12 media and treated for 4 h or 24 h in DMEM/F12 media (supplemented with 1% P/S) with or without 5% serum. For THP-1 M0 exposures, cells were seeded at 1.0 × 10<sup>5</sup> cells/cm<sup>2</sup> in cRPMI media and treated for 24, 48, and 72 h in cRPMI media.

**Endotoxin Assessment.** Since endotoxins may interfere with the functional immunoassays, the potential presence of endotoxins in the sample preparations was assessed using the Multi-test Limulus Amebocyte Lysate (LAL) pyrogen plus test (Lonza, N594-03) (Gel Cloth LAL assay endogenous endotoxin content ≤ 0.003 EU/mL). Serial two-fold dilutions of each sample were tested until an endpoint was reached. SPIONs@SiO<sub>2</sub>-PDA were compared to an internal standard control corresponding to decreasing endotoxin concentrations with positive (high concentration of endotoxin) and negative control (H<sub>2</sub>O LAL as pyrogen-free water). The lysate sensitivity was calculated by determining the geometric mean of the endpoint. Each endpoint value was converted to log<sub>10</sub>. The individual log<sub>10</sub> values were averaged, and the lysate sensitivity was taken as the antilog<sub>10</sub> of this average log value.

**AlamarBlue Assay.** The alamarBlue assay was used to evaluate the metabolic activity of A549 cells. The exposure medium was removed, and A549 cells were washed once with DPBS 1X without CaCl<sub>2</sub> and MgCl<sub>2</sub> (Gibco, 14190-094) before adding 500 μL of pre-warmed fresh exposure media (DMEM/F12 + 1% P/S with or without 5% FBS) containing 10% PrestoBlue HS Cell Viability Reagent (Thermo Fisher Scientific, A13262). After an incubation of 1 h at 37 °C in 5% CO<sub>2</sub>, the fluorescence (Ex 565 nm; Em 590 nm) was measured using the Varioskan LUX plate reader equipped with SkanIt Software 4.1 for Microplate Readers RE, ver. 4.1.0.43 (MULTISKAN SKY Microplate Spectrophotometer, Thermo Fisher Scientific). Background fluorescence (PrestoBlue solutions in medium with or without serum) was subtracted from each well, and data were normalized to the control cells. Data from three independent experiments are expressed as mean ± standard error mean (SEM).

**Lactate Dehydrogenase Assay.** The Lactate Dehydrogenase (LDH) assay was used to assess the cytotoxicity in A549 cells by measuring the LDH leakage into the cell culture media upon plasma membrane disruption. After the exposure, supernatants from each well were collected, and the assay was carried out using the LDH activity kit (Roche, S-11644793001) with 100 μL of the supernatant following the supplier's instructions. Untreated cells were incubated for 20 min with 0.2% Triton-X (Sigma-Aldrich, 9036-19-5) and used as positive controls (PC). Absorbance at 490 and 630 nm was recorded with a Varioskan LUX plate reader provided with SkanIt Software 4.1 for Microplate Readers RE, ver. 4.1.0.43 (Thermo Fisher Scientific). The absorbance values of the background controls (medium with or without serum) were removed from each sample. The results from three independent experiments are expressed as LDH (%) = [(average of treated cell values – lowest control value)/(average of positive control – lowest control value) × 100] and the corresponding SEM. The lowest control value corresponds to spontaneous LDH activity, while the positive control represents the maximum.

**Colony Forming Efficiency Assay.** The colony forming efficiency (CFE) assay was applied to measure the clonogenicity of A549 cells upon treatment. The exposure medium was removed, and cells were washed once with DPBS. Cells were trypsinized with a 0.05% trypsin–EDTA solution (Sigma-Aldrich, T4174) for 1 min at RT, and the trypsin–EDTA solution was removed, and the cells were incubated for another 3 min at 37 °C. Cells were then resuspended in 500 μL of 5% FBS DMEM/F12 media and centrifuged for 7 min at 200g with a Heraeus Fresco17 microcentrifuge (Thermo Fisher Scientific) at 4 °C. The supernatant was discharged, and cells were resuspended in 300 μL of complete media (5% FBS). Cells were diluted 1:1 with Trypan Blue (Logos Bio, T13001) and counted with a Neubauer chamber (Marienfeld). Cells were finally seeded at 300 cells/well in 6-well plates in duplicates for each treatment. The medium was changed every two days. After 10 days, cells were fixed with 3.5% (v/v) of formaldehyde solution (Carl Roth, 4980.1) in DPBS 1X without CaCl<sub>2</sub> and MgCl<sub>2</sub> and stained with 10% (v/v) Giemsa solution (PanReac AppliChem, 251337) in Milli-Q water. Colonies composed of at least 50 cells were counted with Fiji software.<sup>30</sup> The results from three independent experiments are expressed as CFE (%) = [(average number of treatment colonies/average number of control colonies) × 100] and the corresponding SEM (*n* = 3).

**Genotoxicity.** Single- and double-strand DNA breaks were assessed using the alkaline mini-gel COMET assay described in Di Bucchianico et al.<sup>31</sup> Briefly, A549 cells were harvested, and 20 μL of cell suspension (250,000 cells/mL) were mixed with 140 μL of 1% low gelling temperature agarose (Sigma-Aldrich, A9414) at 37 °C. 20 μL aliquots were loaded as drops onto microscopy slides coated with 0.5% standard gelling temperature agarose (Sigma-Aldrich, 05066). Mini-gels underwent 1 h of lysis, followed by 40 min of alkaline treatment and subsequent electrophoretic separation for 25 min (270–300 mA, 1.2 V/cm<sup>2</sup>). Slides were neutralized by washing twice with 0.4 M Tris (Carl Roth, A411.1) and once with ultrapure water. The slides were air-dried at least overnight, and DNA was stained with SYBR GOLD (Invitrogen, S7563) in a 1:10,000 dilution. Pictures were taken with a fluorescence microscope (20× magnification, BioTek Lionheart FX), and CometScore 2.0 software (TriTek Corp) was used to manually score 50 nucleoids per mini-gel. Two mini-gels per sample were prepared, and three independent exposures were performed. Results were expressed as the mean ± DNA in tail ± SEM (*n* = 3). Cells treated with 30 μM hydrogen peroxide (H<sub>2</sub>O<sub>2</sub>, Merck, Darmstadt, Germany, 107209) for 5 min on ice were used as a positive control.

**Malondialdehyde Quantification.** Malondialdehyde (MDA) content, an end product of lipid peroxidation, was measured to investigate oxidative stress. After the exposure, 80 μL of each well's supernatant was collected and frozen at –80 °C. Samples were analyzed by LC–MS/MS according to an already published method without modifications.<sup>32</sup> MDA contents (ng/mL) were normalized with the metabolic cell equivalents (MCE)<sup>33</sup> derived from the LDH data of the corresponding treatment wells and expressed as the mean of two independent experiments, each with two technical replicates, ± SEM (*n* = 2).

**MTS Assay.** THP-1 cell viability was determined in vitro by the 3-(4,5-dimethylthiazol-2-yl)-5-(3-carboxymethoxyphenyl)-2-(4-sulphophenyl)-2H-tetrazolium MTS assay, using the CellTiter 96 Aqueous One Solution Cell Proliferation Assay kit (Promega, G3582) according to the manufacturer's protocol. After the exposure, 20 μL of MTS solution was added, and the cells were further incubated under the same conditions for an additional 2 h. The absorbance of the dissolved formazan was measured with an automated microplate reader (Imark Plate Reader, BioRad) at 490 nm. Cell viability percentage was determined as the ratio between the absorbance (OD) of treated and control cells × 100. Control cells were defined as cells treated with the medium only.

**Tumor Necrosis Factor Alpha Quantification.** The PMA-differentiated naïve M(0) THP-1 macrophages were seeded in 48-well tissue cultures at a concentration of 6 × 10<sup>5</sup> cells/mL. After 24 h without PMA stimulus, cells were incubated with SPIONs@SiO<sub>2</sub>-

PDA at different concentrations for 24 or 48 h at 37 °C and 5% CO<sub>2</sub>. The cells were stimulated with 10 ng/mL Lipopolysaccharide (LPS) (*Escherichia coli* O55:B5, Sigma-Aldrich) as a positive control. Following 24 and 48 h exposures, supernatants were collected and stored at -80 °C until analysis. An enzyme-linked immunosorbent assay (ELISA) was performed following the manufacturer's instructions (Invitrogen, BMS223INST). Tumor necrosis factor alpha (TNF- $\alpha$ ) production was evaluated in three independent experiments performed in duplicate.

**Hemolysis Assay.** Heparinized blood samples were obtained from three healthy human subjects. SPIONs@SiO<sub>2</sub>-PDA was added to an 8% human erythrocyte solution and incubated at 37 °C for 30 min. The samples were centrifuged at 2000g for 5 min, and the supernatant absorbance was measured at 415 nm through the iMark Microplate Absorbance Reader (BioRad, Hercules) to determine the percentage of hemolysis. Triton X-100 1% solution and 1× PBS were taken as 100 and 0% of hemoglobin release, respectively. The haemolysis percentage was determined as the ratio between the OD of treated cells and positive control cells.

**Flow Cytometry-Based Basophil Activation Test.** Heparinized peripheral blood was obtained from 4 volunteers, and SPIONs@SiO<sub>2</sub>-PDA potential allergenic activity was studied by basophil activation in whole blood samples by flow cytometry detecting the combination of the CCR3 and CD63 markers. Blood aliquots (100  $\mu$ L) were incubated with SPIONs@SiO<sub>2</sub>-PDA dilutions in cRPMI for 15 min at 37 °C. PBS and anti-FcEpsilonRI were used as negative and positive controls, respectively. Basophils were detected, as previously reported in Bonura et al.<sup>34</sup> The study was approved by the local Ethics Committee (Comitato Etico Palermo 1, 24 February 2021, resolution n. 02/2021).

**Confocal Microscopy.** A549 cells were seeded on 12 mm-sized coverslips as 45000 cells in 150  $\mu$ L of complete media. After 24 h, cells were exposed to 50  $\mu$ g/mL (corresponding to 13, 16  $\mu$ g/cm<sup>2</sup>) in media with or without 5% serum for 4 and 24 h. The culture media were removed at each endpoint, cells were washed with DPBS without CaCl<sub>2</sub> and MgCl<sub>2</sub>, and then fixed with a 3.5% formaldehyde solution for 15 min at RT. Cells were washed twice with 0.05% Tween-20 (Chem Cruz, K0316) in DPBS (washing buffer) and permeabilized with 0.2% Triton X-100 (Sigma-Aldrich, 7BJ3924) in DPBS for 15 min at RT. After two other washing steps in DPBS, unspecific binding was blocked with 1% BSA and 0.1% Triton-X 100 (blocking buffer) in DPBS for 30 min at RT. The cytoskeleton was stained with Alexa594 phalloidin (1:40 in blocking buffer; Thermo Fisher Scientific, A12381) for 1 h at RT. Slides were washed three times with washing buffer and further incubated with NucGreen Dead 488 (3 drops in 1.5 mL H<sub>2</sub>O; Invitrogen, R37109) for 15 min. Coverslips were washed three times with the washing buffer and then embedded by using mounting medium (Glycergel, DAKO, Agilent, C056330-2). 1636  $\times$  1636 pixel images were acquired with a Zeiss LSM880 with a C-Apochromat 63 $\times$ /1.20 W Korr M27 objective.

**Inductively Coupled Plasma Atomic Emission Spectroscopy.** A549 nanoparticles uptake, iron release from the SPIONs@SiO<sub>2</sub>-PDA in cell medium, and the total added iron content were quantified using inductively coupled plasma atomic emission spectroscopy (ICP-AES). A549 cells were seeded at 1.82  $\times$  10<sup>4</sup> cells/cm<sup>2</sup> for the 4 and 24 h treatments and at 1.56  $\times$  10<sup>4</sup> cells/cm<sup>2</sup> for the 48 h treatment in 6-well tissue culture plates (Corning, 3524). After 24 h, cells were exposed to 10 or 50  $\mu$ g/mL SPIONs@SiO<sub>2</sub>-PDA dispersions (corresponding to 2.1 and 10.4  $\mu$ g/cm<sup>2</sup>) prepared in DMEM/F12 media (supplemented with 1% P/S) with or without 5% serum as described above. For cellular uptake studies, at the end of the exposure, A549 cells were washed twice with PBS, harvested, counted, and finally resuspended in 2 mL of DMEM/F12 media with or without 5% FBS. For iron release in the cell medium, the conditioned media were collected and centrifuged at 13,000 rpm for 1 h at 4 °C to pellet dispersed SPIONs@SiO<sub>2</sub>-PDA, and the supernatant was carefully recovered. To measure the total amount of added iron, dispersions with concentrations of 10 and 50  $\mu$ g/mL were also prepared. Then, ICP-AES analysis was performed on samples diluted 1:3 with Milli-Q water. An ICP-AES ARCOS (Spectro Ametek, Kleve,

Germany) was used for iron determination using the spectral element line of 259.941 nm. Sample introduction was carried out by a peristaltic pump connected to a micromist nebulizer with a cyclon spray chamber. The radio frequency (RF) power was set to 1400 W, the plasma gas was 15 L Ar/min, whereas the nebulizer gas was 0.6 L Ar/min. Regularly, after 10 measurements, three blank determinations and a control determination of a certified standard were performed. The calculation of results was carried out on a computerized lab-data management system, relating the sample measurements to calibration curves, blank determinations, and control standards.

**Assays In Vivo in *C. elegans*.** Nematodes have been grown and handled following standard procedures under uncrowded conditions on nematode growth medium (NGM) agar plates seeded with *E. coli* strain OP50.<sup>35</sup> Strains used in this work have been provided by the *Caenorhabditis* Genetics Center (CGC), which is funded by the NIH Office of Research Infrastructure Programs (P40 OD010440): wild-type strain N2, Bristol variety; CL2166 *dvIs19* [(pAF15) *pgst-4::GFP::NLS*] that expresses an oxidative stress-responsive GFP. Animal treatments with SPIONs@SiO<sub>2</sub>-PDA and Milli-Q water as mock were performed *in iquid* in 96-multiwell plates for the entire life-cycle of the animals (chronic treatment).<sup>36</sup> Synchronized eggs, obtained by bleaching, were resuspended in M9 buffer (3 g KH<sub>2</sub>PO<sub>4</sub>; 6 g Na<sub>2</sub>HPO<sub>4</sub>; 5 g NaCl; 1 M mgSO<sub>4</sub>; H<sub>2</sub>O to 1 L) with 2 $\times$  antibiotic/antimycotic solution (Sigma-Aldrich, A5955), 5 ng/mL cholesterol and OP50. 60  $\mu$ L containing ~30 eggs were aliquoted in each well. SPIONs@SiO<sub>2</sub>-PDA solutions were prepared for animal treatment as described before, diluted in Milli-Q water, and added to the solution containing the animals at the final concentrations of 0.01, 0.1, 1, 10, and 50  $\mu$ g/mL for the thrashing assay and 50  $\mu$ g/mL for brood size, embryonic lethality, SWIP, and *pgst-4::GFP* expression. To evaluate SPIONs@SiO<sub>2</sub>-PDA effects on brood size and embryonic lethality, 20 hermaphrodite animals at the L4 stage treated as described above were transferred to new plates every 24 h for all the fertile period of the animals (4 days), and the number of laid and hatched eggs were counted every day. Treatments were performed twice and in triplicate. To test SPIONs@SiO<sub>2</sub>-PDA effect on animal movement, a thrashing assay was performed on young adult hermaphrodite animals transferred in 7  $\mu$ L of M9 buffer. Animals were left 5 min in a buffer and then video recorded for 30 s. The measurement of thrashing was done by counting every change of direction with respect to the longitudinal axis of the body. Treatments were performed twice and in triplicate. Swimming-induced paralysis (SWIP) assay was performed to test a putative effect of polydopamine on animal motility.<sup>37</sup> Hermaphrodite animals were cleaned from bacteria by allowing them to crawl on an empty plate for 5 min before each experiment. 10 young adult hermaphrodite animals were placed into 40  $\mu$ L of M9 buffer in a watch glass, and their paralysis was scored after 10 min. Treatments were performed in triplicate. *pgst-4::GFP* expression was quantified after treatment when hermaphrodite animals reached the young adult stage. Five animals were transferred onto each glass slide with a 4% agar pad and immobilized alive for microscopy analysis with 100 mM NaN<sub>3</sub> (Sigma-Aldrich, S8032).<sup>38</sup> Epi-fluorescence images were collected with a Leica TCS SP8 AOBS inverted microscope, using a 10 $\times$  objective and FITC filter. Fluorescence quantification was performed using ImageJ, and the corrected total fluorescence (CTF) was calculated for each image: (integrated density of the area containing the animals) - [(area containing the animals)  $\times$  (mean fluorescence of the background)]. For all the experiments, the sample size was determined considering the estimated variability of similar experiments reported in the literature and of previous experiments performed in the laboratory. Animals have been divided by simple randomization, since all animals originate from one plate with thousands of animals that are isogenic and clonal siblings from self-fertilizing homozygous hermaphrodites; no inclusion or exclusion criteria have been set, and all animals scored have been included. To minimize potential confounders, we standardized treatment conditions by simultaneously treating animals with mock and SPIONs@SiO<sub>2</sub>-PDA in the same 96-well plate. We performed a blind quantification when the *pgst-4::GFP* expression was evaluated by ImageJ software that provides unbiased data analysis. No

blind analysis has been performed in other experiments, considering the complex manipulation of animals required to perform them. No primary outcome measure has been used in this study. All animal experiments comply with the ARRIVE guidelines and the U.K. Animals (Scientific Procedures) Act, 1986, and associated guidelines and with EU Directive 2010/63/EU for animal experiments.

**Statistical Analysis.** For A549 toxicity screening, statistical analysis was performed using GraphPad Prism software with a regular two-way analysis of variance (ANOVA) followed by the Tukey multiple comparison test. All comparisons were considered significant when  $p$  was  $< 0.05$ . For the *in vivo* experiments in *C. Elegans*, non-parametric tests (one-way ANOVA Kruskal–Wallis test and Mann–Whitney  $t$ -test) were used for statistical analyses performed with GraphPad Prism, and no relevant assumption has been tested. The effect size was calculated by dividing the difference between the two groups (the mean of the treatment group minus the mean of the control group) by the pooled standard deviation (Cohen's  $d$  formula with a 95% confidence interval).

## RESULTS AND DISCUSSION

### Silica-Coating and Polydopamine Functionalization.

The effectiveness of the silica coating and the polydopamine surface functionalization was confirmed by X-ray diffraction (XRD), FTIR, and FESEM-EDX elemental composition spectrum. In Figure 1b, the diffraction peaks at  $2\theta = 18.80$ ,  $30.01$ ,  $35.60$ ,  $43.51$ ,  $53.78$ ,  $57.46$ ,  $62.97$ ,  $71.41$ , and  $74.54^\circ$  can be assigned to (1 1 1), (2 2 0), (3 1 1), (4 0 0), (4 2 2), (5 1 1), (4 4 0), (6 2 0), and (5 5 3) planes by comparison with the International Centre for Diffraction Data (ICDD no. 00-019-629), which correspond with an inverse spinel structure crystalline phase of magnetite.<sup>39</sup> In addition, we observed a broad band located between  $15$  and  $30^\circ$  (blue pattern), representing the distinguishing feature of the amorphous nature of silica shells.<sup>40</sup> In Figure 1c, SPIONs@SiO<sub>2</sub>-PDA (blue pattern) and SPIONs@OA (black pattern) FTIR spectra showed similar bands around  $580\text{ cm}^{-1}$ , attributed to the stretching vibration mode associated with the metal–oxygen Fe–O bonds in the crystalline lattice of Fe<sub>3</sub>O<sub>4</sub>.<sup>41</sup> For SPIONs@OA,  $2915$ ,  $2843$ ,  $1513$ , and  $1409\text{ cm}^{-1}$  bands corresponded to the stretching vibrations of CH<sub>2</sub> (asymmetric and symmetric) and the stretching modes (asymmetric COO<sup>-</sup> and symmetric COO<sup>-</sup>) of the oleic acid.<sup>41</sup> On the other hand, in SPIONs@SiO<sub>2</sub>-PDA spectra, the silica coating was further confirmed by the appearance of three peaks at  $960$ ,  $440$ , and  $810\text{ cm}^{-1}$ , corresponding to the stretching modes of Si–O–Si (asymmetric and symmetric) and the scissoring vibration of Si–O–Si, respectively. In addition, PDA functionalization was demonstrated by the presence of absorption bands at  $3370$ ,  $2936$ ,  $2869$ ,  $1503$ ,  $1432$ , and  $1340\text{ cm}^{-1}$ , associated with –NH stretching, –CH<sub>2</sub> (asymmetric and symmetric), –C=N stretching, –NH bending, and –C–N–C stretching vibrations, respectively.<sup>42</sup> In addition, FESEM-EDX elemental composition spectrum analysis of SPIONs@SiO<sub>2</sub>-PDA (Figure 1d,e) clearly confirmed the presence of iron, silicon, oxygen, and nitrogen. It has to be highlighted that nitrogen corresponds to the functionalization of PDA carrying functional groups (–NH) on its surface. This fact corroborates the presence of PDA on the SPIONs@SiO<sub>2</sub> and the absence of other elements, indicating the high purity of the prepared nanoparticles. An additional carbon peak appears to have originated from the carbon sample holders (Figure 1e).

**Morphological, Optical, and Magnetic Characterizations.** SPIONs@SiO<sub>2</sub>-PDA displayed spherical morphologies ranging in size around  $20\text{ nm}$  (Figure 2a,b) with magnetite

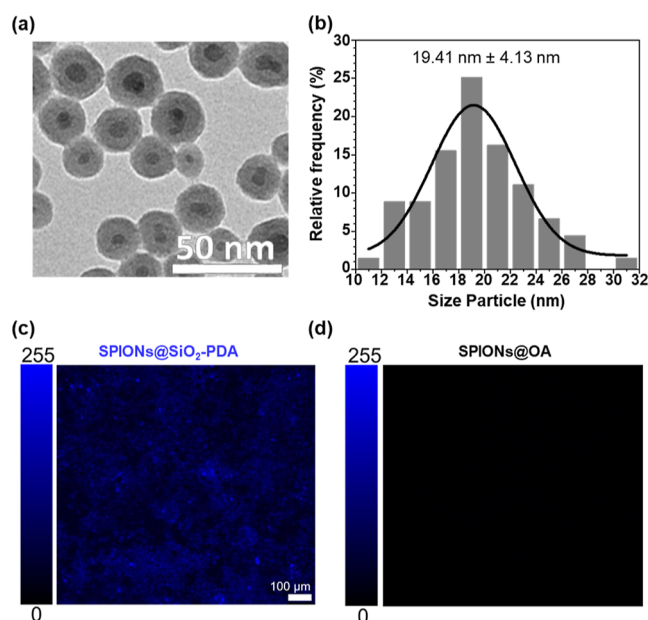


**Figure 2.** Morphological and optical properties of SPIONs@SiO<sub>2</sub>-PDA. (a) Representative TEM picture of SPIONs@SiO<sub>2</sub>-PDA; (b) size distribution (nm) of SPIONs@SiO<sub>2</sub>-PDA performed with Image J software with  $N = 400$  nanoparticles; (c,d) confocal fluorescence images of (c) SPIONs@SiO<sub>2</sub>-PDA and (d) SPIONs@OA with fluorescence intensity scales on the left (RFU).

cores (dark contrast) embedded inside a remarkable silica coating, differently from what was observed with uncoated SPIONs@OA, which showed an irregular spherical shape with an average size of around  $10\text{ nm}$  (Figure S2a,b). For further details, see Supporting Information). SPIONs@SiO<sub>2</sub>-PDA presented a blue-colored fluorescent signal, confirming the presence of fluorescent PDA on the surface, while no signals were observed for SPIONs@OA (Figure 2c,d).

SPIONs@OA NPs and SPIONs@SiO<sub>2</sub>-PDA presented negligible coercive fields ( $H_C = 3.5$  and  $3.4\text{ Oe}$ , respectively) and remanence ( $M_R = 0.6\text{ emu/g}_{\text{Fe}_3\text{O}_4}$ ), corresponding to superparamagnetic behavior at room temperature (Figure S2c–e). In addition, the saturation magnetization of  $M_{\text{sat}}^{\text{NP}} = 63.7\text{ emu/g}_{\text{Fe}_3\text{O}_4}$  below the bulk magnetite value ( $92\text{ emu/g}_{\text{Fe}_3\text{O}_4}$ ) was consistent with a surface inactive magnetic layer, a characteristic signature of the small size of the particles.<sup>43</sup> SPIONs@SiO<sub>2</sub>-PDA magnetic properties were assessed under an applied magnetic field of  $100\text{ Oe}$  in the field-cooled (FC) and zero-field-cooled (ZFC) regimes as a function of temperature (Figure 3a). The ZFC curve reached its maximum at about  $84\text{ K}$ , which corresponds to the blocking temperature ( $T_B$ ) of the particles.<sup>44,45</sup> In contrast, at temperatures higher than  $84\text{ K}$ , they are in a superparamagnetic (SPM) regime since magnetization can randomly flip directions under the influence of temperature and their time-averaged value is zero when there is no external field. In contrast, at temperatures higher than  $84\text{ K}$ , they are in a superparamagnetic (SPM) regime since magnetization can randomly flip directions under the influence of temperature and their time-averaged value is zero when there is no external field.

The remarkable magnetic properties of SPIONs@SiO<sub>2</sub>-PDA indicate their potential use as vehicles for drug delivery or hyperthermia treatments. Indeed, they can be effectively concentrated and confined in submillimeter-wide regions by

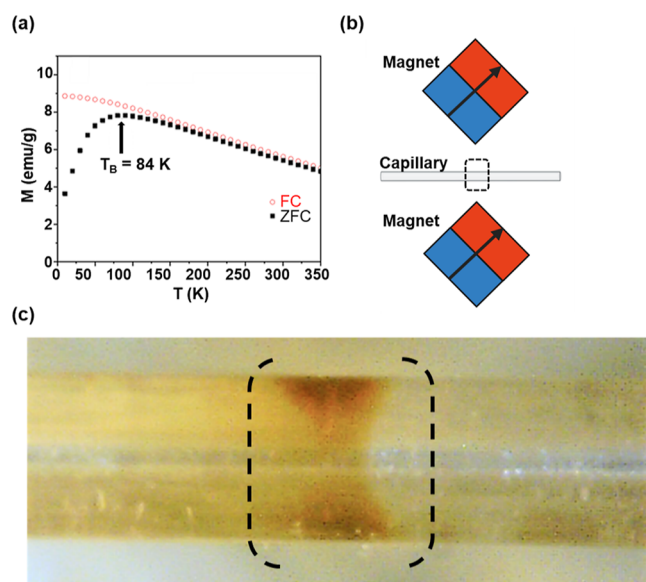


**Figure 3.** SPIONs@SiO<sub>2</sub>-PDA magnetic characterization and experimental realization of confinement by permanent magnets (a) ZFC and FC magnetization curves measured under an applied magnetic field of 100 Oe; (b) sketch of the experimental device described in the text; dashed square shows the position where the image in (c) is taken from; (c) SPION@SiO<sub>2</sub>@PDA concentrated into a clepsydra-shaped region spanning across the entire capillary section.

a specially designed arrangement of commercial static magnets. It is composed of a couple of cubic  $5 \times 5 \times 5 \text{ mm}^3$  NdFeB permanent magnets with a remanence field of 1.3 T, spaced by 5 mm and oriented as shown in Figure 3b. A transparent 500  $\mu\text{m}$  wide quartz capillary, placed at the mid-point between the magnets, allows optical inspection of the magnetic concentration. After a uniform solution of 1 mg/mL of SPION@SiO<sub>2</sub>@PDA in deionized water (18 M $\Omega$ ) was introduced in the capillary, the nanoparticles got concentrated (in ca. 10 min) into a stable configuration between the magnets. It consists of two lobes at the capillary's walls united by a sharp vertex in the middle of the capillary (Figure 3c). It is worth noticing here that, since the nanoplateforms can be easily collected by a magnetic field, as experimentally demonstrated here, this can eliminate the cumbersome centrifugation procedures for collecting them.

**Colloidal Stability and Physicochemical Properties in Cell Culture Media.** Understanding NP's behavior in biological media is the first line of developing safe and effective nanomaterials. In complex biological solutions, NPs interact with the biomolecules presented in the media before getting in touch with cells. Fetal bovine serum (FBS) is a necessary supplement for cell culturing and is usually used to mirror a physiological environment in biological assays. FBS-derived constituents can affect NP physicochemical properties, influencing their biological performances.<sup>46</sup> For these reasons, we investigated SPIONs@SiO<sub>2</sub>-PDA behavior in media with or without serum regarding colloidal stability and physicochemical properties (e.g., hydrodynamic diameter). Since cell culture media composition can vary according to the different cell types, DLS measurements were carried out in the two different cell culture media used for the biological in vitro assays, namely RPMI and DMEM:F12 with and without FBS. Data revealed that—once immersed in FBS-containing media

(complete media)—SPIONs@SiO<sub>2</sub>-PDA z-averaged hydrodynamic diameter  $D_z$  appeared 20 and 25% (cRPMI and cDMEM/F12, respectively) higher when compared to the size in water, likely due to the formation of an enhanced bio-corona around NPs (Table 1). On the other hand, SPIONs@SiO<sub>2</sub>-

**Table 1.** Physicochemical Properties of SPIONs@SiO<sub>2</sub>-PDA in Culture Media<sup>a</sup>

solvent	diameter $z$ nm	PDI
water	$105 \pm 5$	0.27
RPMI	$105 \pm 5$	0.27
DMEM/F12	$105 \pm 5$	0.27
cRPMI	$120 \pm 10$	0.19
cDMEM/F12	$120 \pm 10$	0.19

<sup>a</sup>z-averaged hydrodynamic diameter  $D_z$  and the polydispersity index (PDI) in different media; the same values were measured at each incubation time (4 and 24 h).

PDA average diameters and size distributions remained unchanged in FBS-free media. It is worth noting that the measured size  $D_z = 105 \text{ nm}$  was larger than the size determined by TEM measurements; these values are comparable if one converts from intensity averaged to number averaged size distribution.<sup>29</sup> DLS was also used to assess the stability of SPIONs@SiO<sub>2</sub>-PDA in different media (S3). Interestingly, a slight fraction of aggregates below 1% was detected after 4 and 24 h of incubation in FBS-free media, indicating a marginal instability in these buffers after long storage (Figure S3a–c). At the same time, no changes in size distributions and stability were observed in complete media after 24 h (S3b–d).

**In Vitro Cytotoxicity and Genotoxicity in the Presence and Absence of Serum.** One of the significant drawbacks contributing to the SPIONs' withdrawal from the market is the activation of unwanted immunological responses.<sup>47</sup> In most cases, immunotoxicity and toxicity can be driven by impurities and pyrogenic contamination derived from the synthetic process. SPIONs@SiO<sub>2</sub>-PDA were analyzed for their endogenous content in LPS. For each sample, serial two-fold dilutions were tested until an endpoint was reached. The obtained values are depicted in Table 2. The endotoxin concentration was expressed as EU/mL for a correlation between the concentration of endotoxins in our materials and the LPS concentration used in the internal standard, showing a small amount of endotoxins' contamination in the range of concentrations used in the following biological assays.

In cell culture media (as well as in biological fluids), NPs come surrounded by proteins and other biomolecules, forming a protein corona (PC) through a reversible process that exchanges over time.<sup>48</sup> It has already been demonstrated that the PC derived from proteins in FBS-containing cell culture media can alter NP colloidal stability,<sup>49</sup> impacting cellular interactions and leading to unexpected toxic effects or impaired intracellular internalization. Cellular uptake, tissue penetration, and toxicity of protein-coated SPIONs differ significantly from the pristine ones,<sup>7,50,51</sup> and an overall analysis in different conditions is required. However, the toxicological effects of the FBS-derived protein corona around the particles are unclear and differ from cell lines.<sup>49,52,53</sup> As expected, we observed that the in vitro toxic effects of SPIONs@SiO<sub>2</sub>-PDA depended on the exposure media characteristics. LDH assay showed mild toxic effects (<10%) in cells exposed for 4 h in both complete and serum-free media (Figure 4a). We observed a slight

**Table 2.** Assessment of Endotoxin Contamination of SPIONs@SiO<sub>2</sub>-PDA Dispersions at the Concentrations Used for the Biological Assays<sup>a</sup>

internal standard controls	NC (H <sub>2</sub> O LAL)	0.0075 EU/mL	0.0125 EU/mL	0.03 EU/mL	0.06 EU/mL	PC 0.6 EU/mL
	–	–	–	+/-	+	+
SPIONs@ SiO <sub>2</sub> -PDA	0.1 μg/mL	0.5 μg/mL	1 μg/mL	5 μg/mL	10 μg/mL	50 μg/mL
	–	–	–	+/-	+	+

<sup>a</sup>+ sign is used to define a positive endotoxin signal (i.e., gel cloth formation), while – or +/- signs are used for samples where the endotoxin level is below the threshold level of detection (0.03 EU/mL). The negative control corresponds to pyrogen-free water and the positive control to the high concentration of endotoxins.

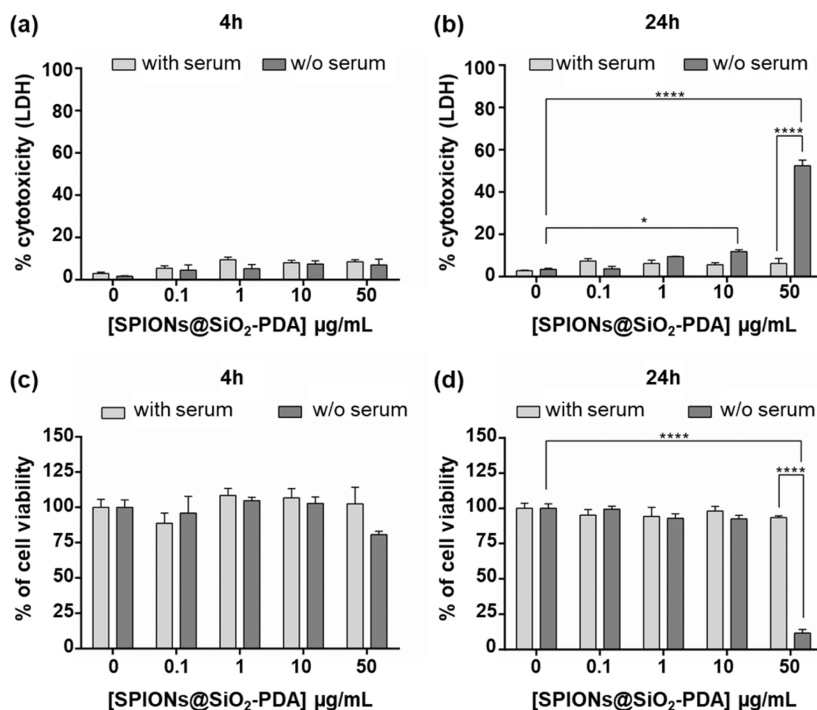


**Figure 4.** In vitro cytotoxicity screening in A549 cells in the presence and absence of serum. (a,b) Cytotoxicity measured by the LDH assay upon 4 h (a) and 24 h (b) exposures ( $n = 3$ ). (c,d) Cell viability measured by the alamarBlue assay after 4 h (c) and 24 h (d) exposure ( $n = 3$ ); legend: \* =  $p \leq 0.05$ , \*\*\*\* =  $p \leq 0.0001$ .

increase in the cytotoxicity levels when cells were treated with 10 μg/mL for 24 h in serum-free media compared to the untreated cells (Figure 4b). As shown in Figure 4b, the highest concentration of SPION dispersions (50 μg/mL) in serum-free media caused a severe and significant increase in cytotoxicity, reaching  $\geq 50\%$  of cell death. No cytotoxicity was observed following 24 h exposures in complete media. Analogously, Reczyńska et al.<sup>54</sup> also obtained no cytotoxic effects in A549 cells exposed to 10 μg/mL silica-coated SPIONs in media supplemented with FBS. Results from the LDH assay were confirmed by the Alamar Blue assay, in which we analyzed the viability of metabolically active cells. Indeed, we did not observe any significant differences in cellular viability after 4 h in both cell exposure conditions at each concentration, consistent with the low amount of LDH leakage (Figure 4c). However, we saw a significant decrease in cell viability of approximately 90-fold in cells treated with 50 μg/mL in serum-free media for 24 h compared to the relative control (Figure 4d).

We also investigated clonogenicity, analyzing the ability of cells to survive and proliferate in colonies up to 10 days post-exposure. Though not statistically significant, we observed a slight decrease in the percentage of clonogenicity in A549 cells treated with all concentrations for 4 h (Figure 5a) and with the

middle concentrations (1 and 10 μg/mL) following 24 h exposure in media with serum (Figure 5b). Cells treated in serum-free media with the lowest (0.1 μg/mL) and middle concentrations showed a mild decrease in clonogenicity after 4 h (Figure 5a) and no significant increase after 24 h with 0.1 and 1 μg/mL treatments (Figure 5b). Cells exposed to the highest concentration (50 μg/mL) for 4 h in serum-free media presented a marked and significant decrease in clonogenicity of approximately 80–70-fold compared to the untreated and the cells treated with the same concentration but in media with serum (Figure 5a). 24 h exposures in serum-free media to the highest concentration caused a severe decrease in clonogenicity of approximately 80–60-fold, although not statistically relevant (Figure 5b). The significant impairment in clonogenicity obtained with the highest concentration in the 4 and 24 h serum-free exposures (Figure 5a,b) might result from single and double DNA strand breaks. Genotoxicity analyses confirmed that SPIONs@SiO<sub>2</sub>-PDA significantly increased strand breaks up to 4.9–8.9% when cells were treated for 4 h (Figure 5c) and 24 h (Figure 5d), respectively. Interestingly, the earlier time point (4 h) also showed significant damage with the 10 μg/mL formulation compared to the untreated cells (4.4% DNA in the tail) (Figure 5c). On the other hand, we did not observe significant genotoxic effects when cells were



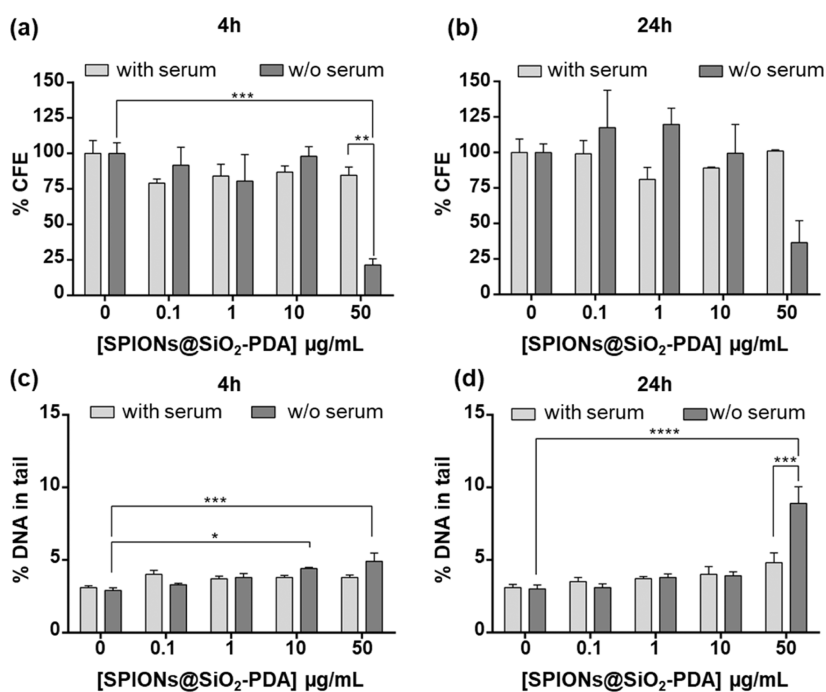


**Figure 5.** In vitro clonogenicity and DNA damage in A549 cells in the presence and absence of serum. (a,b) Cytotoxicity measured by clonogenicity with the CFE assay in cells treated for 4 h (a) and 24 h (b) ( $n = 3$ ). (c,d) DNA damage upon 4 h treatment (c) and 24 h (d) treatment. Legend: \* =  $p \leq 0.05$ , \*\*\* =  $p \leq 0.001$ , \*\*\*\* =  $p \leq 0.0001$ .

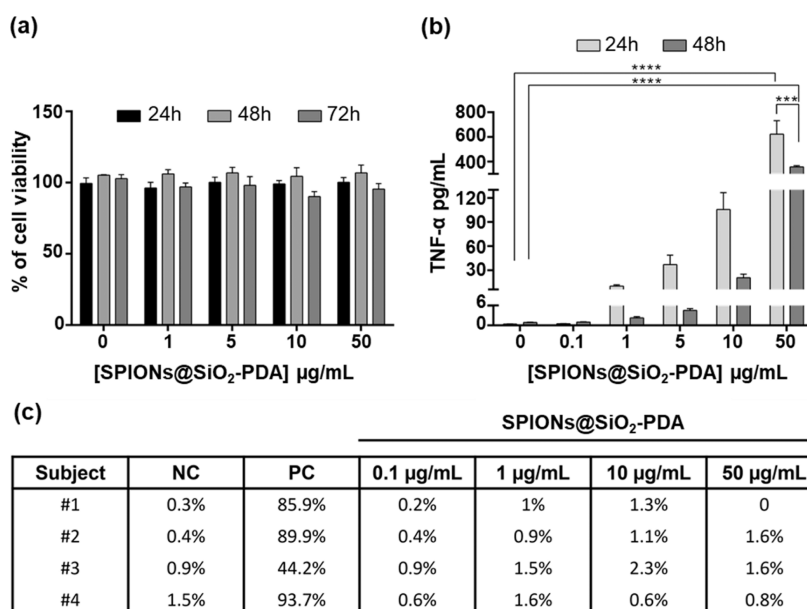


**Figure 6.** In vitro and ex vivo immunotoxicity screening. (a) Immunotoxicity measured by the MTS assay upon 24, 48, and 72 h ( $n = 3$ ); (b) TNF- $\alpha$  release measured by ELISA following 24 and 48 h exposure; (c) human basophil activation.

treated in complete media at distinct time points and concentrations. In sum, both cytotoxic and genotoxic data confirmed the high biocompatibility of SPIONs@SiO<sub>2</sub>-PDA once immersed in FBS-containing media at each time point and concentration.

**In Vitro and Ex Vivo Immunotoxicity.** Immunotoxicity was evaluated in the THP-1 cell line with a M0 macrophage-like phenotype in media supplemented with FBS. As for A549 cells, SPIONs@SiO<sub>2</sub>-PDA did not affect cell viability after 24 and 48 h for all the tested concentrations, but we observed a mild effect (<10%) following 72 h exposures at the highest

concentration (Figure 6a). However, after 24 h exposure, SPIONs@SiO<sub>2</sub>-PDA induced a progressive release of TNF- $\alpha$  with increasing nanoparticles concentrations, significant at 50 µg/mL, whereas a remarkable decrease (up to 8 times) was observed after 48 h (Figure 6b). The increased TNF- $\alpha$  release along with the tested concentrations could be enhanced by the positive endotoxin contamination observed for concentrations higher than 10 µg/mL. In order to further address such immunotoxicity drawbacks, we studied the potential allergenicity of the SPIONs by applying an ex vivo assay using whole blood from healthy subjects ( $n = 4$ ) in an attempt to detect

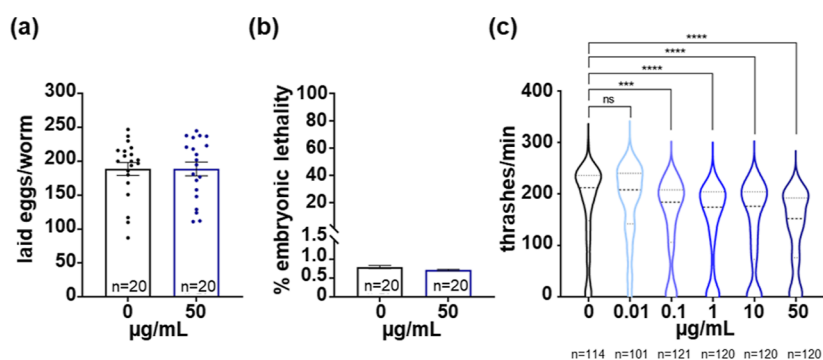


**Figure 7.** In vivo toxicity screening. (a) Effect of SPIONs@SiO<sub>2</sub>-PDA (SPIONs) on egg deposition. Each dot represents the number of laid eggs per P<sub>0</sub> worm in the fertile period of the animal; *n* is the number of P<sub>0</sub> parental animals analyzed. (b) Effect of SPIONs@SiO<sub>2</sub>-PDA on embryonic survival. The percentage of unhatched eggs on the total number of laid eggs was calculated. Bars represent the mean and error bar is the SEM. *n* is the number of P<sub>0</sub> parental animals analyzed. (c) Effect of SPIONs@SiO<sub>2</sub>-PDA on animal movement. Violin plots show the distribution of thrashes performed by the animals in a minute. Bold dashed line in the center corresponds to the median, while the upper and lower dashed lines correspond to the quartiles. *n* is the number of total animals analyzed. Legend: ns corresponds to *p* > 0.9999; \*\*\* to *p* < 0.0005; \*\*\*\**p* < 0.0001 (one-way ANOVA Kruskal–Wallis test).

possible immediate basophil activation. Our data indicated that SPIONs@SiO<sub>2</sub>-PDA did not display the ability to activate human basophil cells per se, showing a percentage of basophil activation similar to the negative control in all tested concentrations (Figure 6c). To corroborate the low ex vivo immunotoxicity on human peripheral blood mononuclear cells (PBMC), we performed a red blood cell hemolysis test (*n* = 3), showing that SPIONs@SiO<sub>2</sub>-PDA did not induce significant lysis of erythrocytes at the tested concentrations (Figure S4).

**In Vivo Toxicity.** The animal model *C. elegans* was used to evaluate SPIONs@SiO<sub>2</sub>-PDA toxicity and bioactivity in the context of a whole living animal, providing insights at the systematic, cellular, and molecular level. Previous work demonstrated that exposure to iron NPs, uncoated or functionalized with different coating materials, can cause lethality, defects in growth and offspring, and defects in animal movement.<sup>55–57</sup> We assessed the effects of the highest concentration (50 µg/mL) on animal fertility after chronic treatment, and, importantly, we did not observe any effect on animal brood size (Figure 7a) nor on embryonic survival (Figure 7b). However, at the same concentration, we observed a slight reduction in animal motility in water, a behavior called thrashing (Figure 7c), similar to what we had previously observed.<sup>56</sup> The biological significance calculated with Cohen's method corresponds to a *d* = 0.68 (lower limit on *d*: 0.49, upper: 0.89), thus suggesting a medium effect size. Moreover, after treating animals with different concentrations of SPIONs@SiO<sub>2</sub>-PDA (0.01, 0.1, 1, and 10 µg/mL), we confirmed a mild reduction of thrashing at all the concentrations used, except for 0.01 µg/mL, with a dose-dependent trend (Figure 7c). Therefore, SPIONs@SiO<sub>2</sub>-PDA are more compatible than other iron-NPs in respect to the fitness of the animal, but still cause a slight defect in locomotion. This interesting feature of SPIONs@SiO<sub>2</sub>-PDA underlines the necessity of testing also locomotion as a more subtle and sensitive assay for assessing nanoparticle toxicity. Importantly, this peculiar aspect deserves further investigation but paves the way for further improvements to enhance SPIONs@SiO<sub>2</sub>-PDA biocompatibility. In *C. Elegans*, alterations in dopamine content affect animal motility. In particular, a reduction in dopamine release causes a defect of thrashing,<sup>58</sup> while an excess of dopamine induces a swimming induced

paralysis (SWIP).<sup>59</sup> Thus, we verified whether polydopamine in SPIONs@SiO<sub>2</sub>-PDA could influence animal motility similarly to an excess of dopamine by performing the SWIP assay on treated animals, and we did not observe any difference when comparing animals treated with mock or SPIONs@SiO<sub>2</sub>-PDA (Figure S5). Thermogravimetric analysis (TGA) revealed that the PDA content is represented by 22% of SPIONs@SiO<sub>2</sub>-PDA weight (Figure S6). These data strongly support for PDA not affecting animal motility per se.

#### In Vitro and In Vivo Oxidative Stress Evaluation.

Oxidative stress represents one of the biggest concerns with the use of SPIONs. After being taken up by cells, SPIONs can be degraded inside lysosomal compartments, releasing free iron ions into the cytoplasm.<sup>7</sup> High levels of free iron ions increase the production of radical oxygen species (ROS), causing the oxidation of several biomolecules, including DNA and lipids. Silica coating has literature precedence in preventing particle intracellular degradation.<sup>11</sup> Still, the presence of proteins around silica-coated SPIONs might have an active role in favoring the degradation of the silica coating and, consequently, the iron ion leakage from the core.<sup>52</sup> Oxidative stress was assessed in vitro by measuring malondialdehyde (MDA) content in the culture media and in vivo in *C. elegans* by evaluating the expression levels of the homolog of the glutathione *S*-transferase, *gst-4*, an essential gene involved in the detoxification process that promotes the oxidative stress resistance.<sup>60,61</sup> MDA is one of the final products of polyunsaturated fatty acid peroxidation in the cells, and it is often used as a marker of lipid peroxidation and oxidative stress. We observed no significant effects following 4 h exposure both in media with and without serum (Figure 8a). 24 h after exposure, MDA levels in cells treated in complete media were relatively lower than what we observed after 4 h exposures, indicating a time-dependent recovery process (Figure 8b). On the other hand, we observed relevant increases in MDA levels after serum-free media treatments when cells were exposed to the higher concentration. In *C. elegans*, exposure to iron NPs can activate the oxidative stress response and ROS accumulation.<sup>56</sup> To evaluate *gst-4* expression levels, we used a transgenic strain expressing GFP under the control of the *gst-4* promoter.<sup>38</sup> After treatments, we observed a significant increase in the expression of *pgst-4::GFP* fluorescence compared to animals treated with mock (Figure

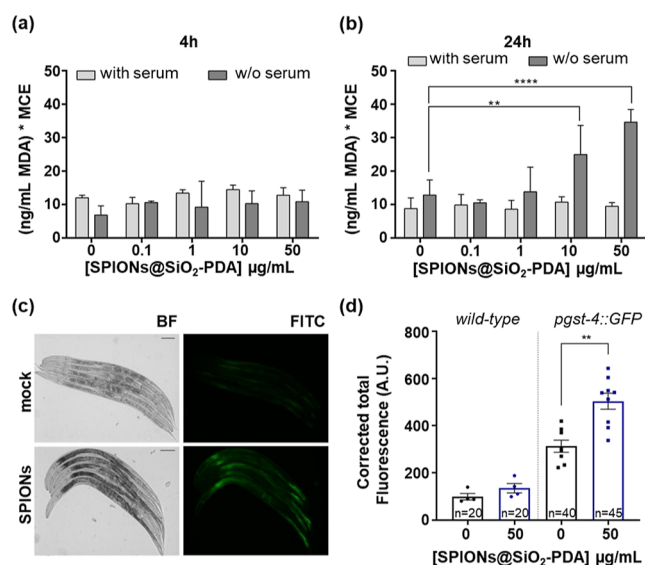


**Figure 8.** Activation of the oxidative stress response in vitro and in vivo. Malondialdehyde (MDA) levels [ng/mL] after 4 h (a) and 24 h (b) in A549 cells exposed to SPIONs@SiO<sub>2</sub>-PDA measured in the supernatant via LC–MS/MS. Data were normalized with the MCE derived from LDH values of the corresponding wells; (c) representative images of *pgst-4:GFP* animals treated with mock (0) (upper panels) and SPIONs@SiO<sub>2</sub>-PDA 50  $\mu\text{g/mL}$  (lower panels) and acquired with bright-field (BF) and epi-fluorescence (FITC) methods. The anterior part of the animal is on the left. Scale bar, 75  $\mu\text{m}$ . (d) Quantification of the fluorescence in wild-type and *pgst-4:GFP* animals, after treatment with no SPIONs (0) or SPIONs@SiO<sub>2</sub>-PDA 50  $\mu\text{g/mL}$ . Wild-type animals were also imaged to exclude any contribution of the intestinal autofluorescence to the analysis. Each dot represents the total fluorescence in the picture corrected for the background (CTF). Bars represent the mean and error bars are SEM. *n* is the total number of animals analyzed. Mann–Whitney *t*-test was used to establish the significance of treated *pgst-4:GFP* animals vs mock. Legend: \*\**p* = 0.0016.

8c,d) and a very large size effect (Cohen's *d* = 1.88, lower limit on *d*: 1.39, upper: 2.36), suggesting that chronic exposure to SPIONs@SiO<sub>2</sub>-PDA can also induce an oxidative stress response in vivo.

**Intracellular Uptake and Iron Release.** Several studies reported that the FBS-derived proteins could also affect cellular uptake and could lead to significant decreases in cellular uptake (Kiliç et al. 2015).<sup>53</sup> Thus, the low cytotoxicity levels observed in our work might be related to a notable decrease in SPIONs@SiO<sub>2</sub>-PDA cellular uptake when dispersed in complete media. To verify this hypothesis, cellular uptake studies were conducted by confocal microscopy and ICP-AES. The cellular uptake efficiency in the presence of serum proteins was markedly lower than for SPIONs@SiO<sub>2</sub>-PDA incubated in serum-free conditions (Figure 9). According to data quantification of confocal images, this phenomenon was particularly evident upon 4 h exposures (Figure S7). The decrease of the PDA fluorescence signal after 24 h exposure might be related to SPIONs degradation upon cellular engulfment. Notably, a certain degree of cytoskeleton disturbance can be observed after short term exposures in both tested conditions (Phalloidin staining, Figure 9). Due to the role of the actin cytoskeleton in endocytosis, its disturbance might explain the minor uptake reduction observed following the shorter time-point exposures in both conditions. This observation is in line with the findings of Francia and co-authors on the complex role of cell receptors, protein corona formation, and actin disruption with inhibitors in the mechanisms used by cells to internalize silica NPs.<sup>62</sup>

SPIONs@SiO<sub>2</sub>-PDA uptake was quantified in terms of iron cellular content and nanoparticle number which were significantly higher following cell exposures in serum-free media, possibly explaining the higher observed toxic effects (Figure 10a,b). Furthermore, the cytotoxicity, genotoxicity, and increased oxidative stress could also be related to a differential iron release from the core of nanoparticles due to silica-coating degradation. However, we could exclude such a

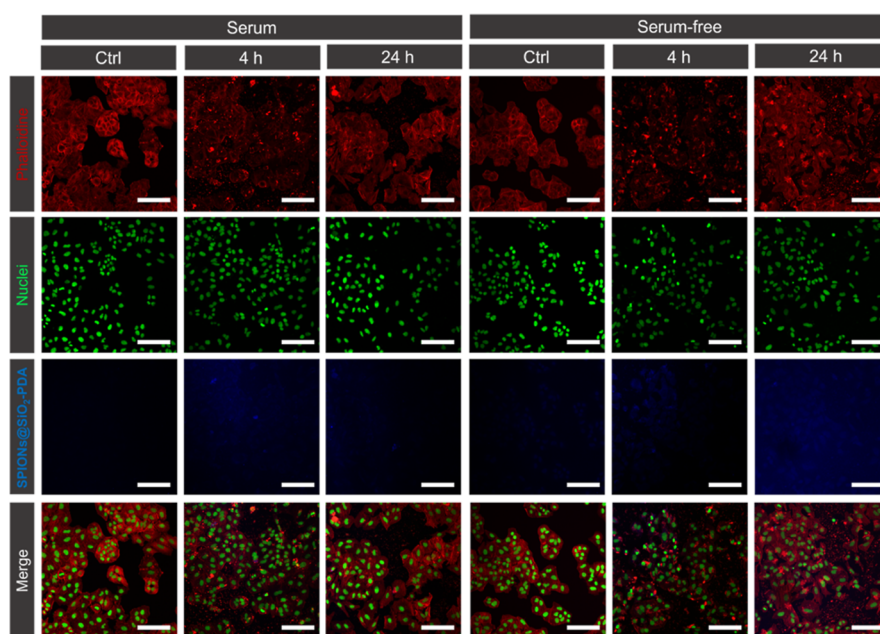


**Figure 9.** Intracellular uptake. Confocal microscopy after 4 and 24 h exposure in A549 cells with 50  $\mu\text{g/mL}$  SPIONs@SiO<sub>2</sub>-PDA in media with and without 5% serum. Actin cytoskeleton was stained with phalloidin, and nuclei were stained with NucGreen Dead 488. Scale bar, 100  $\mu\text{m}$ .

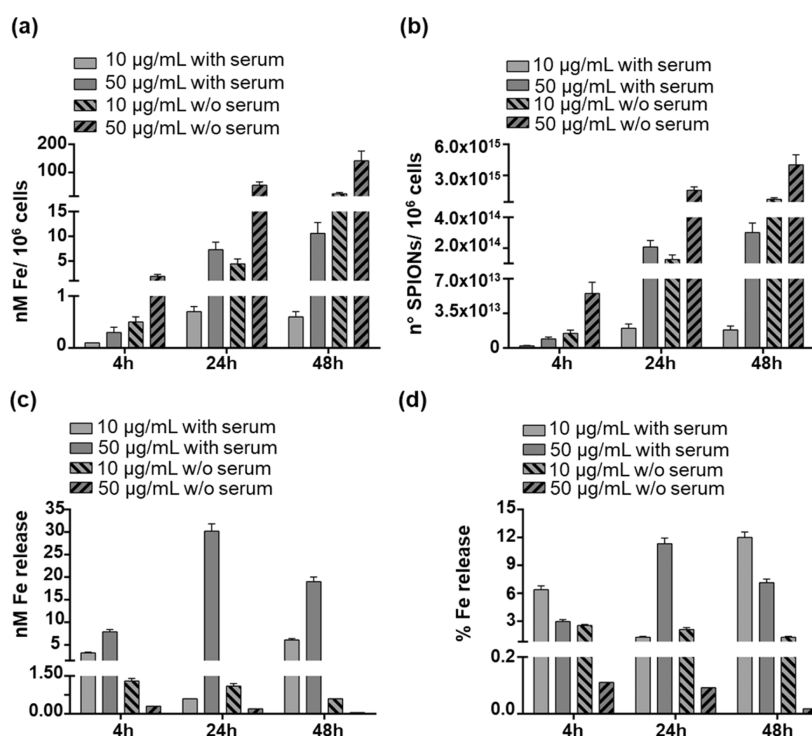


**Figure 10.** Intracellular uptake and iron release. ICP-AES analysis after 4, 24, and 48 h exposure in A549 cells with 10 or 50 µg/mL SPIONs@SiO<sub>2</sub>-PDA in media with and without 5% serum. (a) nanomolar iron cellular uptake; (b) number of SPIONs@SiO<sub>2</sub>-PDA cellular uptake; (c) nanomolar iron release into culture media; (d) percentage of iron released into culture media compared to the total added iron content. Data are expressed as mean ± RSD.

hypothesis since the release of iron was generally detected at the nM level (Figure 10c) and was negligible in serum-free exposures (<2% of total added iron, Figure 10d), probably due to the higher instability of SPIONs@SiO<sub>2</sub>-PDA and their tendency to form aggregates as shown by DLS measurements in serum-free media. Notably, the diminished PDA fluorescence signals noticed by confocal microscopy imaging followed 24 h exposures (Figure S7) might be explained by the increased iron release at the same exposure time (Figure 10c). Overall, these aspects are of particular importance for the potential use of the developed SPIONs@SiO<sub>2</sub>-PDA nanoplat-form for nanomedicine purposes since in vivo NPs encounter much higher serum concentrations compared to in vitro scenario, and further studies are needed.

## CONCLUSIONS

SPIONs' clinical application is hindered by several limitations related to safety and toxicity concerns. In the last few years, the implementation of safe-by-design approaches to discover novel biocompatible shells has contributed to minimizing SPION toxicity. However, the flexibility in their synthetic route and the absence of gold standard methods often result in complex bio-nano interactions that are difficult to predict. As such, a comprehensive and systematic biological characterization—from in vitro to in vivo—is needed to assess toxicity risks and efficacies. In this study, we developed biocompatible silica-coated SPIONs functionalized with PDA with magnetic and fluorescent features. SPIONs@SiO<sub>2</sub>-PDA were physicochemically characterized by complementary techniques, defining the shape, morphology, and magnetic properties. SPIONs@SiO<sub>2</sub>-PDA showed high stability in culture media supplemented with FBS, foreseeing their colloidal behavior in more complex true-to-life biological fluids. SPIONs@SiO<sub>2</sub>-PDA proved to be

biocompatible in vitro in FBS-containing media, ex vivo in whole blood exposure, and in vivo in the invertebrate animal model *C. elegans*. Furthermore, the possibility of confining them in submillimeter-wide regions paves the way for their implementation for theranostic applications.

## ASSOCIATED CONTENT

### Supporting Information

The Supporting Information is available free of charge at <https://pubs.acs.org/doi/10.1021/acsbomaterials.2c00946>.

Chemical details of the synthesis of silica-coated SPIONs functionalized with polydopamine; morphological and magnetic characterization of the SPIONs@OA precursor; DLS measurements; hemolytic potential in whole human blood samples; SWIP assay on animals treated with mock or SPIONs@SiO<sub>2</sub>-PDA; TGA; and fluorescence intensity quantification of confocal imaging (PDF)

## AUTHOR INFORMATION

### Corresponding Author

Sebastiano Di Bucchianico — Joint Mass Spectrometry Center (JMSC) at Comprehensive Molecular Analytics, Helmholtz Zentrum München, Neuherberg 85764, Germany; [orcid.org/0000-0002-6396-892X](https://orcid.org/0000-0002-6396-892X); Email: [dibucchianico@helmholtz-muenchen.de](mailto:dibucchianico@helmholtz-muenchen.de)

### Authors

Miriam Romano — Department of Molecular and Translational Medicine, University of Brescia, Brescia 25123, Italy; Center for Colloid and Surface Science (CSGI), Florence 50019, Italy; Joint Mass Spectrometry Center

(JMASC) at Comprehensive Molecular Analytics, Helmholtz Zentrum München, Neuherberg 85764, Germany; [orcid.org/0000-0002-3972-460X](https://orcid.org/0000-0002-3972-460X)

**Manuel Antonio González Gómez** – NANOMAG Laboratory, Applied Physics Department, iMATUS Materials Institute, Universidade de Santiago de Compostela, Santiago de Compostela 15782, Spain

**Pamela Santonicola** – Institute of Biosciences and BioResources (IBBR), National Research Council of Italy (CNR), Naples 80131, Italy; [orcid.org/0000-0002-4094-9996](https://orcid.org/0000-0002-4094-9996)

**Noemi Aloï** – Institute for Biomedical Research and Innovation (IRIB), National Research Council of Italy (CNR), Palermo 90146, Italy; [orcid.org/0000-0002-6424-8588](https://orcid.org/0000-0002-6424-8588)

**Svenja Offer** – Joint Mass Spectrometry Center (JMASC) at Comprehensive Molecular Analytics, Helmholtz Zentrum München, Neuherberg 85764, Germany

**Jana Pantzke** – Joint Mass Spectrometry Center (JMASC) at Comprehensive Molecular Analytics, Helmholtz Zentrum München, Neuherberg 85764, Germany

**Samuele Raccosta** – Institute of Biophysics (IBF), National Research Council of Italy (CNR), Palermo 90146, Italy

**Valeria Longo** – Institute for Biomedical Research and Innovation (IRIB), National Research Council of Italy (CNR), Palermo 90146, Italy

**Alessandro Surpi** – Institute of Nanostructured Materials (ISMN), National Research Council of Italy (CNR), Bologna 40129, Italy

**Silvia Alacqua** – Department of Molecular and Translational Medicine, University of Brescia, Brescia 25123, Italy; Center for Colloid and Surface Science (CSGI), Florence 50019, Italy; Joint Mass Spectrometry Center (JMASC) at Comprehensive Molecular Analytics, Helmholtz Zentrum München, Neuherberg 85764, Germany

**Giuseppina Zampi** – Institute of Biosciences and BioResources (IBBR), National Research Council of Italy (CNR), Naples 80131, Italy

**Valentin Alek Dediu** – Institute of Nanostructured Materials (ISMN), National Research Council of Italy (CNR), Bologna 40129, Italy

**Bernhard Michalke** – Research Unit Analytical BioGeoChemistry, Helmholtz Zentrum München, Neuherberg 85764, Germany

**Ralf Zimmerman** – Joint Mass Spectrometry Center (JMASC) at Comprehensive Molecular Analytics, Helmholtz Zentrum München, Neuherberg 85764, Germany

**Mauro Manno** – Institute of Biophysics (IBF), National Research Council of Italy (CNR), Palermo 90146, Italy; [orcid.org/0000-0001-9843-0428](https://orcid.org/0000-0001-9843-0428)

**Yolanda Piñeiro** – NANOMAG Laboratory, Applied Physics Department, iMATUS Materials Institute, Universidade de Santiago de Compostela, Santiago de Compostela 15782, Spain; [orcid.org/0000-0003-4614-1629](https://orcid.org/0000-0003-4614-1629)

**Paolo Colombo** – Institute for Biomedical Research and Innovation (IRIB), National Research Council of Italy (CNR), Palermo 90146, Italy

**Elia Di Schiavi** – Institute of Biosciences and BioResources (IBBR), National Research Council of Italy (CNR), Naples 80131, Italy

**José Rivas** – NANOMAG Laboratory, Applied Physics Department, iMATUS Materials Institute, Universidade de

Santiago de Compostela, Santiago de Compostela 15782, Spain; [orcid.org/0000-0002-5059-3196](https://orcid.org/0000-0002-5059-3196)

**Paolo Bergese** – Department of Molecular and Translational Medicine, University of Brescia, Brescia 25123, Italy; Center for Colloid and Surface Science (CSGI), Florence 50019, Italy; [orcid.org/0000-0002-4652-2168](https://orcid.org/0000-0002-4652-2168)

Complete contact information is available at:

<https://pubs.acs.org/10.1021/acsbmaterials.2c00946>

## Author Contributions

M.R.: conceptualization, validation, formal analysis, investigation, data curation, writing—original draft, writing—review and editing, visualization; M.A.G.G., N.A., S.O., J.P., S.R., V.L., S.A., B.M.: validation, formal analysis, investigation, data curation; writing—original draft; P.S., A.S.: conceptualization, methodology, validation, software, writing—original draft, visualization, formal analysis, investigation, data curation; G.Z.: resources, investigation, project administration; V.A.D., R.Z.: resources, supervision; M.M., Y.P., P.C., E.D.S., J.R.: conceptualization, resources, writing—reviewing and editing, supervision, funding acquisition; P.B., S.D.B.: conceptualization, formal analysis, resources, writing—reviewing and editing, supervision, project administration, funding acquisition.

## Notes

The authors declare no competing financial interest.

## ACKNOWLEDGMENTS

This work was supported by the VES4US and the BOW projects funded by the European Union's Horizon 2020 research and innovation programme, under grant agreements nos 801338 and 952183; this work was also partially supported by the National Research Council (Seed DISBA-CNR Prize 2021) (E.D.S.).

## REFERENCES

- (1) Wu, K.; Su, D.; Liu, J.; Saha, R.; Wang, J. P. Magnetic nanoparticles in nanomedicine: a review of recent advances. *Nanotechnology* **2019**, *30*, 502003.
- (2) Xiáng, Y.; Idée, J. M. A comprehensive literature update of clinical researches of superparamagnetic resonance iron oxide nanoparticles for magnetic resonance imaging. *Quant. Imag. Med. Surg.* **2017**, *7*, 88–122.
- (3) Piñeiro, Y.; Vargas, Z.; Rivas, J.; López-Quintela, M. A. Iron Oxide Based Nanoparticles for Magnetic Hyperthermia Strategies in Biological Applications. *Eur. J. Inorg. Chem.* **2015**, *2015*, 4495–4509.
- (4) Wahajuddin, M.; Arora, A. Superparamagnetic iron oxide nanoparticles: Magnetic nanoplatforms as drug carriers. *Int. J. Nanomed.* **2012**, *7*, 3445–3471.
- (5) Schubert, J.; Chanana, M. Coating Matters: Review on Colloidal Stability of Nanoparticles with Biocompatible Coatings in Biological Media, Living Cells and Organisms. *Curr. Med. Chem.* **2018**, *25*, 4553–4586.
- (6) Vakili-Ghartavol, R.; Momtazi-Borojeni, A. A.; Vakili-Ghartavol, Z.; Aiyelabegan, H. T.; Jaafari, M. R.; Rezayat, S. M.; Arbabi Bidgoli, S. A. Toxicity assessment of superparamagnetic iron oxide nanoparticles in different tissues. *Artif. Cell Nanomed. Biotechnol.* **2020**, *48*, 443–451.
- (7) Nelson, N.; Port, J.; Pandey, M. Use of Superparamagnetic Iron Oxide Nanoparticles (SPIONs) via Multiple Imaging Modalities and Modifications to Reduce Cytotoxicity: An Educational Review. *J. Nanotheranostics* **2020**, *1*, 105–135.
- (8) Wei, H.; Hu, Y.; Wang, J.; Gao, X.; Qian, X.; Tang, M. Superparamagnetic iron oxide nanoparticles: Cytotoxicity, metabo-

- lism, and cellular behavior in biomedicine applications. *Int. J. Nanomed.* **2021**, *16*, 6097–6113.
- (9) Mojica Pisciotto, M. L.; Lima, E.; Vasquez Mansilla, M.; Tognoli, V. E.; Troiani, H. E.; Pasa, A. A.; Creczynski-Pasa, T. B.; Silva, A. H.; Gurman, P.; Colombo, L.; Goya, G. F.; Lamagna, A.; Zysler, R. D. In vitro and in vivo experiments with iron oxide nanoparticles functionalized with DEXTRAN or polyethylene glycol for medical applications: Magnetic targeting. *J. Biomed. Mater. Res., Part B* **2014**, *102*, 860–868.
- (10) Zavisova, V.; Koneracka, M.; Gabelova, A.; Svitkova, B.; Ursinyova, M.; Kubovcikova, M.; Antal, I.; Khmara, I.; Jurikova, A.; Molcan, M.; Ognjanović, M.; Antić, B.; Kopcansky, P. Effect of magnetic nanoparticles coating on cell proliferation and uptake. *J. Magn. Magn. Mater.* **2019**, *472*, 66–73.
- (11) Malvindi, M. A.; De Mattei, V.; Galeone, A.; Brunetti, V.; Anyfantis, G. C.; Athanassiou, A.; Cingolani, R.; Pompa, P. P. Toxicity assessment of silica coated iron oxide nanoparticles and biocompatibility improvement by surface engineering. *PLoS One* **2014**, *9*, No. e85835.
- (12) Liu, X.; Cao, J.; Li, H.; Li, J.; Jin, Q.; Ren, K.; Ji, J. Mussel-Inspired Polydopamine: A Biocompatible and Ultrastable Coating for Nanoparticles in Vivo. *ACS Nano* **2013**, *7*, 9384–9395.
- (13) Jin, A.; Wang, Y.; Lin, K.; Jiang, L. Nanoparticles modified by polydopamine: Working as ‘drug’ carriers. *Bioact. Mater.* **2020**, *5*, 522–541.
- (14) Siminzar, P.; Omid, Y.; Golchin, A.; Aghanejad, A.; Barar, J. Targeted delivery of doxorubicin by magnetic mesoporous silica nanoparticles armed with mucin-1 aptamer. *J. Drug Targeting* **2020**, *28*, 92–101.
- (15) Singh, N.; Sallem, F.; Mirjolet, C.; Nury, T.; Sahoo, S. K.; Millot, N.; Kumar, R. Polydopamine modified superparamagnetic iron oxide nanoparticles as multifunctional nanocarrier for targeted prostate cancer treatment. *Nanomaterials* **2019**, *9*, 138.
- (16) Iacoviță, C.; Fizeșan, I.; Nitica, S.; Florea, A.; Barbu-Tudoran, L.; Dudric, R.; Pop, A.; Vedeau, N.; Crisan, O.; Teteau, R.; Loghin, F.; Lucaciu, C. M. Silica Coating of Ferromagnetic Iron Oxide Magnetic Nanoparticles Significantly Enhances Their Hyperthermia Performances for Efficiently Inducing Cancer Cells Death In Vitro. *Pharmaceutics* **2021**, *13*, 2026.
- (17) Iqbal, M. Z.; Ma, X.; Chen, T.; Zhang, L.; Ren, W.; Xiang, L.; Wu, A. Silica-coated super-paramagnetic iron oxide nanoparticles (SPIONPs): a new type contrast agent of T1 magnetic resonance imaging (MRI). *J. Mater. Chem. B* **2015**, *3*, 5172–5181.
- (18) Liao, N.; Wu, M.; Pan, F.; Lin, J.; Li, Z.; Zhang, D.; Wang, Y.; Zheng, Y.; Peng, J.; Liu, X.; Liu, J. Poly (dopamine) coated superparamagnetic iron oxide nanocluster for noninvasive labeling, tracking, and targeted delivery of adipose tissue-derived stem cells. *Sci. Rep.* **2016**, *6*, 18746.
- (19) Quignard, S.; d’Ischia, M.; Chen, Y.; Fattaccioli, J. Ultraviolet-Induced Fluorescence of Polydopamine-Coated Emulsion Droplets. *ChemPlusChem* **2014**, *79*, 1254–1257.
- (20) Madhurakkat Perikamana, S. K.; Lee, J.; Lee, Y. B.; Shin, Y. M.; Lee, E. J.; Mikos, A. G.; Shin, H. Materials from Mussel-Inspired Chemistry for Cell and Tissue Engineering Applications. *Biomacromolecules* **2015**, *16*, 2541–2555.
- (21) Faria, M.; Björnalm, M.; Thurecht, K. J.; Kent, S. J.; Parton, R. G.; Kavallaris, M.; Johnston, A. P. R.; Gooding, J. J.; Corrie, S. R.; Boyd, B. J.; Thordarson, P.; Whittaker, A. K.; Stevens, M. M.; Prestidge, C. A.; Porter, C. J. H.; Parak, W. J.; Davis, T. P.; Crampin, E. J.; Caruso, F. Minimum information reporting in bio-nano experimental literature. *Nat. Nanotechnol.* **2018**, *13*, 777–785.
- (22) González-Gómez, M. A.; Belderbos, S.; Yañez-Vilar, S. M.; Piñeiro, Y.; Cleeren, F.; Bormans, G.; Deroose, C. M.; Gsell, W.; Himmelreich, U.; Rivas, J. Development of Superparamagnetic Nanoparticles Coated with Polyacrylic Acid and Aluminum Hydroxide as an Efficient Contrast Agent for Multimodal Imaging. *Nanomaterials* **2019**, *9*, 1626.
- (23) Moldes-Diz, Y.; Gamallo, M.; Eibes, G.; Vargas-Osorio, Z.; Vazquez-Vazquez, C.; Feijoo, G.; Lema, J. M.; Moreira, M. T. Development of a Superparamagnetic Laccase Nanobiocatalyst for the Enzymatic Biotransformation of Xenobiotics. *J. Environ. Eng.* **2018**, *144*, 04018007.
- (24) Schmitz, K. S.; Phillies, G. D. J. *An Introduction to Dynamic Light Scattering by Macromolecules*; Academic Press, 1990.
- (25) Poon, C. Measuring the density and viscosity of culture media for optimized computational fluid dynamics analysis of in vitro devices. *J. Mech. Behav. Biomed. Mater.* **2022**, *126*, 105024.
- (26) Romancino, D. P.; Buffa, V.; Caruso, S.; Ferrara, I.; Raccosta, S.; Notaro, A.; Campos, Y.; Noto, R.; Martorana, V.; Cupane, A.; Giallongo, A.; d’Azzo, A.; Manno, M.; Bongiovanni, A. Palmitoylation is a post-translational modification of Alix regulating the membrane organization of exosome-like small extracellular vesicles. *Biochim. Biophys. Acta Gen. Subj.* **2018**, *1862*, 2879–2887.
- (27) Paterna, A.; Rao, E.; Adamo, G.; Raccosta, S.; Picciotto, S.; Romancino, D.; Noto, R.; Touzet, N.; Bongiovanni, A.; Manno, M. Isolation of Extracellular Vesicles From Microalgae: A Renewable and Scalable Bioprocess. *Front. Biotechnol.* **2022**, *10*, 836747.
- (28) Rausch, K.; Reuter, A.; Fischer, K.; Schmidt, M. Evaluation of Nanoparticle Aggregation in Human Blood Serum. *Biomacromolecules* **2010**, *11*, 2836–2839.
- (29) Adamo, G.; Fierli, D.; Romancino, D. P.; Picciotto, S.; Barone, M. E.; Aranyos, A.; Božič, D.; Morsbach, S.; Raccosta, S.; Stanly, C.; Paganini, C.; Gai, M.; Cusimano, A.; Martorana, V.; Noto, R.; Carotta, R.; Librizzi, F.; Randazzo, L.; Parkes, R.; Capasso Palmiero, U. C.; Rao, E.; Paterna, A.; Santonicola, P.; Igljč, A.; Corcuera, L.; Kisslinger, A.; Di Schiavi, E.; Liguori, G. L.; Landfester, K.; Kralj-Igljč, V.; Arosio, P.; Pocsfalvi, G.; Touzet, N.; Manno, M.; Bongiovanni, A. Nanoalgsomes: Introducing extracellular vesicles produced by microalgae. *J. Extracell. Vesicles* **2021**, *10*, No. e12081.
- (30) Schindelin, J.; Arganda-Carreras, I.; Frise, E.; Kaynig, V.; Longair, M.; Pietzsch, T.; Preibisch, S.; Rueden, C.; Saalfeld, S.; Schmid, B.; Tinevez, J. I.; White, D. J.; Hartenstein, V.; Eliceiri, K.; Tomancak, P.; Cardona, A. Fiji: an open-source platform for biological-image analysis. *Nat. Methods* **2012**, *9*, 676–682.
- (31) Di Bucchianico, S.; Cappellini, F.; Le Bihanic, F.; Zhang, Y.; Dreij, K.; Karlsson, H. L. Genotoxicity of TiO<sub>2</sub> nanoparticles assessed by mini-gel comet assay and micronucleus scoring with flow cytometry. *Mutagenesis* **2017**, *32*, 127–137.
- (32) Cao, C.; Padoan, S.; Binder, S.; Bauer, S.; Orasche, J.; Rus, C. M.; Mudan, A.; Huber, A.; Kuhn, E.; Oeder, S.; Lintelmann, J.; Adam, T.; Di Bucchianico, S.; Zimmermann, R. A comparative study of persistent DNA oxidation and chromosomal instability induced in vitro by oxidizers and reference airborne particles. *Mutat. Res., Genet. Toxicol. Environ. Mutagen.* **2022**, *874*–875, 503446.
- (33) Heinrich, P.; Diehl, U.; Förster, F.; Braunbeck, T. Improving the in vitro ethoxyresorufin-O-deethylase (EROD) assay with RTL-W1 by metabolic normalization and use of  $\beta$ -naphthoflavone as the reference substance. *Comp. Biochem. Physiol., Part C: Toxicol. Pharmacol.* **2014**, *164*, 27–34.
- (34) Bonura, A.; Passantino, R.; Costa, M. A.; Montana, G.; Melis, M.; Luisa Bondi, M. L.; Butteroni, C.; Barletta, B.; Corinti, S.; Felice, G.; Colombo, P. Characterization of a Par j 1/Par j 2 mutant hybrid with reduced allergenicity for immunotherapy of Parietaria allergy. *Clin. Exp. Allergy* **2012**, *42*, 471–480.
- (35) Brenner, S. The genetics of *Caenorhabditis elegans*. *Genetics* **1974**, *77*, 71–94.
- (36) Picciotto, S.; Santonicola, P.; Paterna, A.; Rao, E.; Raccosta, S.; Romancino, D. P.; Noto, R.; Touzet, N.; Manno, M.; Di Schiavi, E.; Bongiovanni, A.; Adamo, G. Extracellular Vesicles From Microalgae: Uptake Studies in Human Cells and *Caenorhabditis elegans*. *Front. Biotechnol.* **2022**, *10*, 830189.
- (37) Lanzo, A.; Safratowich, B. D.; Kudumala, S. R.; Gallotta, I.; Zampi, G.; Di Schiavi, E.; Carvelli, L. Silencing of Syntaxin 1A in the Dopaminergic Neurons Decreases the Activity of the Dopamine Transporter and Prevents Amphetamine-Induced Behaviors in *C. elegans*. *Front. Physiol.* **2018**, *9*, 576.

- (38) Link, C. D.; Johnson, C. J. Reporter Transgenes for Study of Oxidant Stress in *Caenorhabditis elegans*. *Methods Enzymol.* **2002**, *353*, 497–505.
- (39) Kolen'ko, Y. V.; Bañobre-López, M.; Rodríguez-Abreu, C.; Carbó-Argibay, E.; Deepak, F. L.; Petrovykh, D. Y.; Cerqueira, M. F.; Kamali, S.; Kovnir, K.; Shtansky, D. V.; Lebedev, O. I.; Rivas, J. High-Temperature Magnetism as a Probe for Structural and Compositional Uniformity in Ligand-Capped Magnetite Nanoparticles. *J. Phys. Chem. C* **2014**, *118*, 28322–28329.
- (40) Chitra, K.; Annadurai, G. Fluorescent Silica Nanoparticles in the Detection and Control of the Growth of Pathogen. *J. Nanotechnol.* **2013**, *2013*, 509628.
- (41) Nalbandian, L.; Patrikiadou, E.; Zaspalis, V.; Patrikidou, A.; Hatzidaki, E.; N. Papandreou, C. Magnetic Nanoparticles in Medical Diagnostic Applications: Synthesis, Characterization and Proteins Conjugation. *Curr. Nanosci.* **2016**, *12*, 455–468.
- (42) Cheng, W.; Fan, F.; Zhang, Y.; Pei, Z.; Wang, W.; Pei, Y. A Facile Approach for Fabrication of Core-Shell Magnetic Molecularly Imprinted Nanospheres towards Hypericin. *Polymers* **2017**, *9*, 135.
- (43) Sato, T.; Iijima, T.; Seki, M.; Inagaki, N. Magnetic properties of ultrafine ferrite particles. *J. Magn. Magn. Mater.* **1987**, *65*, 252–256.
- (44) Liu, C.; Zou, B.; Rondinone, A. J.; Zhang, Z. J. Chemical Control of Superparamagnetic Properties of Magnesium and Cobalt Spinel Ferrite Nanoparticles through Atomic Level Magnetic Couplings. *J. Am. Chem. Soc.* **2000**, *122*, 6263–6267.
- (45) Bruvera, I. J.; Mendoza Zélis, P.; Pilar Calatayud, M. P.; Goya, G. F.; Sánchez, F. H. Determination of the blocking temperature of magnetic nanoparticles: The good, the bad, and the ugly. *J. Appl. Phys.* **2015**, *118*, 184304.
- (46) Moore, T. L.; Rodriguez-Lorenzo, L.; Hirsch, V.; Balog, S.; Urban, D.; Jud, C.; Rothen-Rutishauser, B.; Lattuada, A.; Petri-Fink, A. Nanoparticle colloidal stability in cell culture media and impact on cellular interactions. *Chem. Soc. Rev.* **2015**, *44*, 6287–6305.
- (47) Patil, R. M.; Thorat, N. D.; Shete, P. B.; Bedge, P. A.; Gavde, S.; Joshi, M. G.; Tofail, S. A. M.; Bohara, R. A. Comprehensive cytotoxicity studies of superparamagnetic iron oxide nanoparticles. *Biochem. Biophys. Rep.* **2018**, *13*, 63–72.
- (48) Auría-Soro, C.; Nesma, T.; Juanes-Velasco, P.; Landeira-Viñuela, A.; Fidalgo-Gomez, H.; Acebes-Fernandez, V.; Gongora, R.; Almendral Parra, M. J.; Manzano-Roman, R.; Fuentes, M. Interactions of nanoparticles and biosystems: Microenvironment of nanoparticles and biomolecules in nanomedicine. *Nanomaterials* **2019**, *9*, 1365.
- (49) Mbeh, D. A.; Javanbakht, T.; Tabet, L.; Merhi, Y.; Maghni, K.; Sacher, E.; Yahia, L. H. Protein Corona Formation on Magnetite Nanoparticles: Effects of Culture Medium Composition, and Its Consequences on Superparamagnetic Nanoparticle Cytotoxicity. *J. Biomed. Nanotechnol.* **2015**, *11*, 828–840.
- (50) Hill, A.; Payne, C. K. Impact of Serum Proteins on MRI Contrast Agents: Cellular Binding and T(2) relaxation. *RSC Adv.* **2014**, *4*, 31735–31744.
- (51) Vogt, C.; Pernemalm, M.; Kohonen, P.; Laurent, S.; Hultenby, K.; Vahter, M.; Lehtiö, J.; Toprak, M. S.; Fadeel, B. Proteomics analysis reveals distinct corona composition on magnetic nanoparticles with different surface coatings: Implications for interactions with primary human macrophages. *PLoS One* **2015**, *10*, No. e0129008.
- (52) Kiliç, G.; Costa, C.; Fernández-Bertólez, N.; Pásaro, E.; Teixeira, J. P.; Laffon, B.; Valdíglesias, V. In vitro toxicity evaluation of silica-coated iron oxide nanoparticles in human SHSY5Y neuronal cells. *Toxicol. Res.* **2016**, *5*, 235–247.
- (53) Balk, M.; Haus, T.; Band, J.; Unterweger, H.; Schreiber, E.; Friedrich, R. P.; Alexiou, C.; Gostian, A. O. Cellular spion uptake and toxicity in various head and neck cancer cell lines. *Nanomaterials* **2021**, *11*, 1–19.
- (54) Reczyńska, K.; Marszałek, M.; Zarzycki, A.; Reczyński, W.; Kornaus, K.; Pamula, E.; Chrzanowski, W. Superparamagnetic iron oxide nanoparticles modified with silica layers as potential agents for lung cancer treatment. *Nanomaterials* **2020**, *10*, 1076.
- (55) Fajardo, C.; Costa, G.; Nande, M.; Martín, C.; Martín, M.; Sánchez-Fortún, S. Heavy metals immobilization capability of two iron-based nanoparticles (nZVI and Fe3O4): Soil and freshwater bioassays to assess ecotoxicological impact. *Sci. Total Environ.* **2019**, *656*, 421–432.
- (56) Wu, Q.; Li, Y.; Tang, M.; Wang, D. Evaluation of Environmental Safety Concentrations of DMSA Coated Fe2O3-NPs Using Different Assay Systems in Nematode *Caenorhabditis elegans*. *PLoS One* **2012**, *7*, No. e43729.
- (57) Gonzalez-Moragas, L.; Yu, S.-M.; Carenza, E.; Laromaine, A.; Roig, A. Protective Effects of Bovine Serum Albumin on Superparamagnetic Iron Oxide Nanoparticles Evaluated in the Nematode *Caenorhabditis elegans*. *ACS Biomater. Sci. Eng.* **2015**, *1*, 1129–1138.
- (58) Mocko, J. B.; Kern, A.; Moosmann, B.; Behl, C.; Hajieva, P. Phenothiazines interfere with dopaminergic neurodegeneration in *Caenorhabditis elegans* models of Parkinson's disease. *Neurobiol. Dis.* **2010**, *40*, 120–129.
- (59) McDonald, P. W.; Hardie, S. L.; Jessen, T. N.; Carvelli, L.; Matthies, D. S.; Blakely, R. D. Vigorous Motor Activity in *Caenorhabditis elegans* Requires Efficient Clearance of Dopamine Mediated by Synaptic Localization of the Dopamine Transporter DAT-1. *J. Neurosci.* **2007**, *27*, 14216–14227.
- (60) Hu, Q.; D'Amora, D. R.; MacNeil, L. T.; Walkout, A. J. M.; Kubiseski, T. J. The *Caenorhabditis elegans* Oxidative Stress Response Requires the NHR-49 Transcription Factor. *G3: Genes, Genomes, Genet.* **2018**, *8*, 3857–3863.
- (61) Oliveira, R. P.; Abate, J. P.; Dilks, K.; Landis, J.; Ashraf, J.; Murphy, C. T.; Blackwell, T. K. Condition-adapted stress and longevity gene regulation by *Caenorhabditis elegans* SKN-1/Nrf. *Aging Cell* **2009**, *8*, 524–541.
- (62) Francia, V.; Yang, K.; Deville, S.; Reker-Smit, C.; Nelissen, I.; Salvati, A. Corona Composition Can Affect the Mechanisms Cells Use to Internalize Nanoparticles. *ACS Nano* **2019**, *13*, 11107–11121.